ELSEVIER

Journal of Structural Geology 26 (2004) 1231–1256

JOURNAL OF STRUCTURAL GEOLOGY

www.elsevier.com/locate/jsg

Structural analysis of faults related to a heterogeneous stress history: reconstruction of a dismembered gold deposit, Stawell, western Lachlan Fold Belt, Australia

John McL. Miller*, Christopher J.L. Wilson

Predictive Mineral Discovery CRC, School of Earth Sciences, The University of Melbourne, Victoria 3010, Australia

Received 24 December 2002; received in revised form 20 July 2003; accepted 4 August 2003

Abstract

In the internationally significant Victorian goldfields a complex system of faults dismembers the 5 million ounce Magdala gold deposit. These faults represent a combination of neoformed faults and inherited faults that reflect deformation associated with stress tensors of variable orientation and stress shape ratio (ϕ). The fault geometry is strongly controlled by the pre-existing rheology. Faults have propagated around the flanks of an antiformal basalt dome, along earlier ductile cleavages and the margins of porphyry dykes. Many of the faults do not have Andersonian geometries and there is no correlation between the orientation of the faults and the palaeostress directions. Much of the faulting is associated with the emplacement of porphyry dykes, additional gold mineralisation related to plutonism and late-stage deformation post-dating the intrusion of the Stawell pluton. Systematic mapping of extension veins associated with faults, striations and conjugate joint sets allowed the construction of a revised and more robust history of brittle deformation. This successfully predicted the offset direction of the currently mined Magdala ore body beneath the studied system of faults. The use of extension veins was a critical aspect of the analysis. If striations on the fault surfaces had solely been used, the offset direction of the new Golden Gift orebody would not have been correctly ascertained. The palaeostress history was delineated via use of compression and tension dihedra, stress inversion of slip data and calculation of theoretical resolved shear stress for faults with orientations similar to those mapped. The calculation of theoretical resolved shear stress directions highlights the importance that the intermediate stress has on the slip direction for faults whose pole does not lie in the plane containing σ_1 and σ_3.

Keywords: Gold; Fault-slip data; Lachlan Fold Belt; Palaeostress

1. Introduction

Structural controls on ore deposits range from the dismemberment of relatively simple stratiform orebodies to orogenic gold located within fault zones. Understanding fault behaviour is critical for understanding ore shoot geometry (e.g. Robert and Poulsen, 2001), the nature of fluid flow and overpressure (Sibson et al., 1988; Cox et al., 1995; Robert et al., 1995; Sibson and Scott, 1998), predicting the location of orebodies offset by late faults (e.g. Miller et al., 2001), and the application of stress modelling (e.g. Holyland and Ojala, 1997; Groves et al., 2000; Cox et al., 2001).

One of the key problems with the structural analysis of fault systems is the problem of heterogeneous data produced by either changes in the orientation of the stress field or the relative magnitudes of the principal stresses through time (e.g. Angelier, 1994; Lisle and Vandycke, 1996; Ramsay and Lisle, 2000). Heterogeneous fault-slip data sets are commonly associated with ancient fault-controlled ore deposits. This paper presents an example of a fault system in the western Lachlan Fold Belt (Fig. 1a and b) that records evidence of a changing stress field associated with plutonism, intrusion-related gold and late-stage post plutonism faulting. The fault system associated with this change in regional stress dismembers one of the largest primary gold deposits within the internationally significant Victorian Goldfields (>5 million ounce endowment; Fredericksen and Gane, 1998; Phillips and Hughes, 1998).

The structural information presented has implications for intrusion-related gold and granite emplacement mechanisms. At a larger scale we provide strong field evidence for a major change in plate convergence in the Late Silurian along the eastern margin of Gondwana. However, the key

* Corresponding author.
E-mail address: jmm@unimelb.edu.au (J.M.L. Miller).

0191-8141/$ - see front matter © 2004 Elsevier Ltd. All rights reserved.
doi:10.1016/j.jsg.2003.11.004

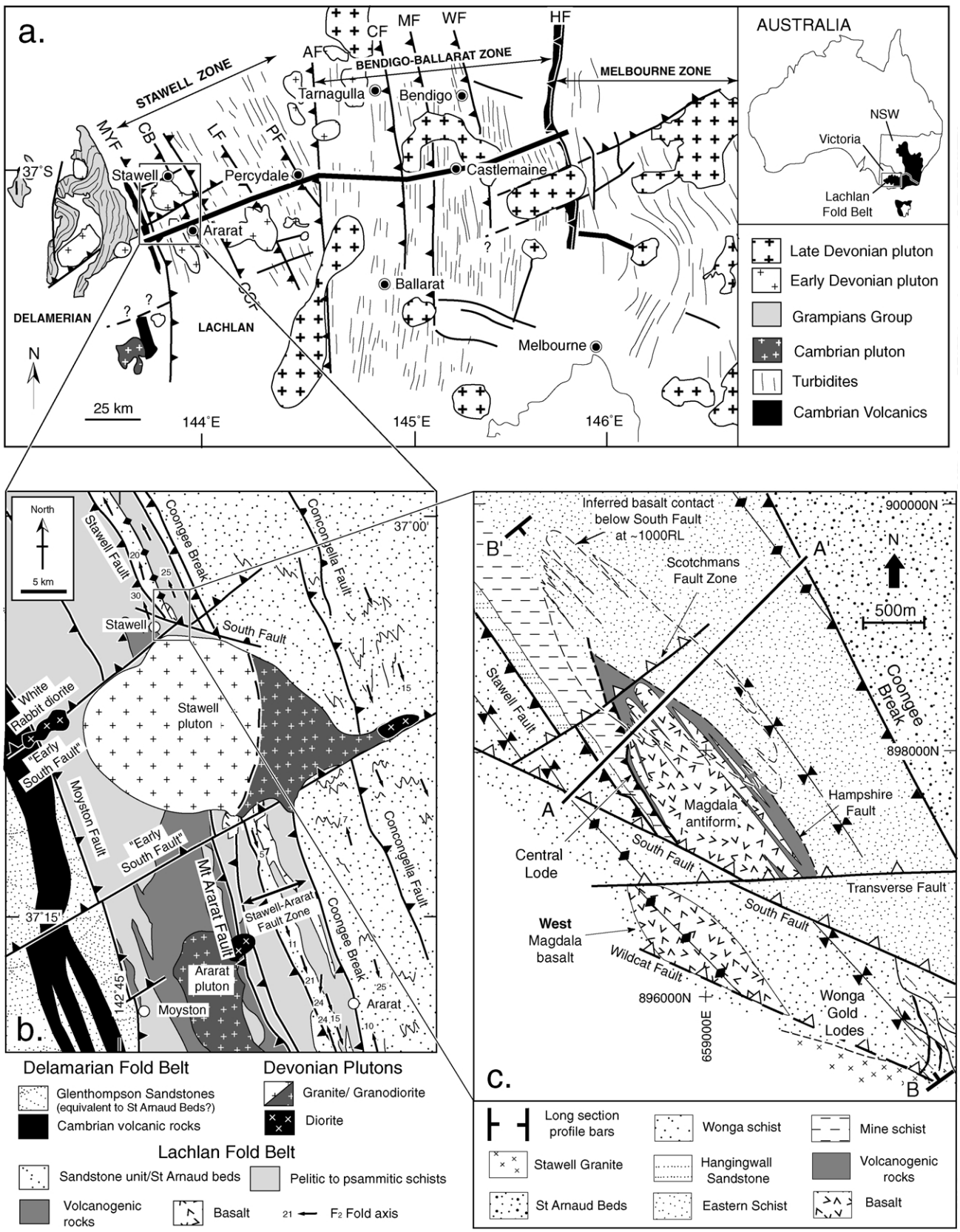

Fig. 1. (a) Geological map of western Victoria (from Miller et al., 2001). Inset shows location of Victoria and New South Wales and extent of Lachlan Fold Belt (black fill). MYF: Moyston Fault; CB: Coongee Break; CCF: Concongella Fault; LF: Landsborough Fault; PF: Percydale Fault; AF: Avoca Fault; CF: Campelltown Fault; MF: Muckleford Fault; WF: Whitelaw Fault; HF: Heathcote Fault. (b) Geological map of the Stawell region (modified from 1:100000

aim of the paper is to present the type of structural information collected from the underground mapping of drive walls, and how these data were utilised via calculation of hanging wall transport directions, the construction of compression and tension dihedra (Angelier, 1984) and stress inversion of the observed fault slip data (using the program SLICK.BAS from Ramsay and Lisle (2000)). This information is combined with calculations of theoretical maximum resolved shear stress directions constructed for variable fault orientations and stress tensors to produce a new structural model consistent with all observed data.

The revised structural model presented in this paper was one of the key pieces of information used by the exploration geologists of Mining Project Investors Pty Ltd to refine the drilling program that recently discovered a major offset portion of the Magdala gold deposit (Figs. 1c and 2a and b; the 'Golden Gift'—Dugdale and Fredericksen, 2000; Miller et al., 2001).

2. Stereographic and palaeostress methods

The underground mapping documented ductile structures, fault/vein arrays, late joints (some of which are Cretaceous in age; Miller et al., 2002) and the mineralogy associated with different vein generations in a series of two-dimensional profiles. The depth of each drive is referred to as a relative level (RL) below the 'Big Hill' reference point (marked on Fig. 2b). Underground data were utilised to calculate the slip sense of all generations of faults by using footwall extension veins and striations—this is represented by an arrow on the stereographic projections (Fig. 3). These arrows indicate the transport direction of the rocks in the hanging wall at the pole to the fault (e.g. Hoeppener, 1955; Oncken, 1988). The slip-direction of a fault is inferred to represent the maximum resolved shear stress on that surface for a given stress tensor (e.g. Ramsay and Lisle, 2000). Slip directions were inferred by utilising striations on the fault surface and extension veins in the direct footwall or hanging wall of a particular fault (e.g. Ramsay and Huber, 1987, p. 536). These directions were represented graphically on equal area stereonets (Fig. 3).

We define the slip direction represented on the stereographic projections (Fig. 3) as the 'hanging wall transport direction'. In the same stress field different hanging wall transport directions can occur for faults with different strike orientations. If two faults have the same orientation, but different hanging wall transport directions, this indicates that there was either a change in the orientation of the principal stresses or a change in their relative magnitudes (or both). The term 'hanging wall transport direction' has been introduced because one of the initial key aims of the structural analysis at Stawell was to delineate the transport direction of the Magdala orebody in the hanging wall of the South Fault system. The base of the orebody is truncated and offset by these faults. For the 'under-the-South-Fault' exploration drilling program (Dugdale and Fredericksen, 2000), determining the transport direction of the *variably* dipping faults was critical. Such nomenclature has little application to strike-slip fault systems.

The simplest case of palaeostress determination is for conjugate faults that formed within the one stress regime (neoformed faults with Andersonian Geometries, e.g. Anderson, 1951; Angelier, 1994). In the case of conjugate faults the delineation of palaeostress directions is simple (Fig. 3e). When pre-existing planes of weakness exist the formation of conjugate systems can be inhibited by the reactivation of variably dipping and striking pre-existing structures producing an 'inherited fault' geometry (e.g. Angelier, 1994).

In this paper we define a fault as having an Andersonian geometry (and also infer it to be neoformed) if its pole lies in the plane containing the inferred palaeostress directions σ_1 and σ_3 and its dip reflects a reasonable orientation compared with that predicted by Mohr–Coloumb theory. For an Andersonian fault geometry (Fig. 3e) the magnitude of intermediate stress (σ_2) does not influence the slip direction on the faults because the intermediate stress axis is parallel to the fault intersection direction (Angelier, 1994). However, this intermediate stress becomes a key factor in defining the slip-direction in the case of inherited faults. Theoretical resolved shear stresses were calculated using the method of Fry (1992). The diagrams of maximum resolved shear stress were used to: (1) demonstrate the shear stress on faults that are not oriented with their pole in the same plane containing σ_1 and σ_3 (non-Andersonian); (2) demonstrate the effects of varying the relative magnitude of σ_2; and (3) demonstrate the effects of a rotating stress field on the resolved shear stress. Instead of complex graphical depictions for an extensive range of stress tensors (e.g. Gómez, 1986), we used a minimal number of fault orientations and stress tensors to provide simple visualisation and qualitative estimates. For these calculations of theoretical shear stress we assumed that one stress is vertical. On these diagrams the shape of the stress tensor is characterized by the relative difference in principal stresses or the stress shape ratio (termed ϕ: $\phi = (\sigma_2 - \sigma_3)/(\sigma_1 - \sigma_3)$; Angelier, 1994). We have only considered the maximum resolved shear stresses a given stress tensor will produce. We have not considered whether the stress tensor

ARARAT and STAWELL, Geological Survey of Victoria map sheets; Cayley and Taylor, 2000a,b). (c) Geological map at −500 RL of the Magdala and Wonga mines. The inferred position of the offset basalt below the South Fault (at about 1000 RL) is marked as a dashed outline. Both the mine and AMG grid northings (and eastings) are marked. The section line and long section for Fig. 2 are also marked. Early mineralising faults have black teeth (e.g. Stawell Fault), later faults that dismember the system, and in some cases further mineralise it, are marked with white teeth (e.g. Scotchmans Fault Zone). Antiform and synform traces to the east and west of the Magdala Antiform are also shown.

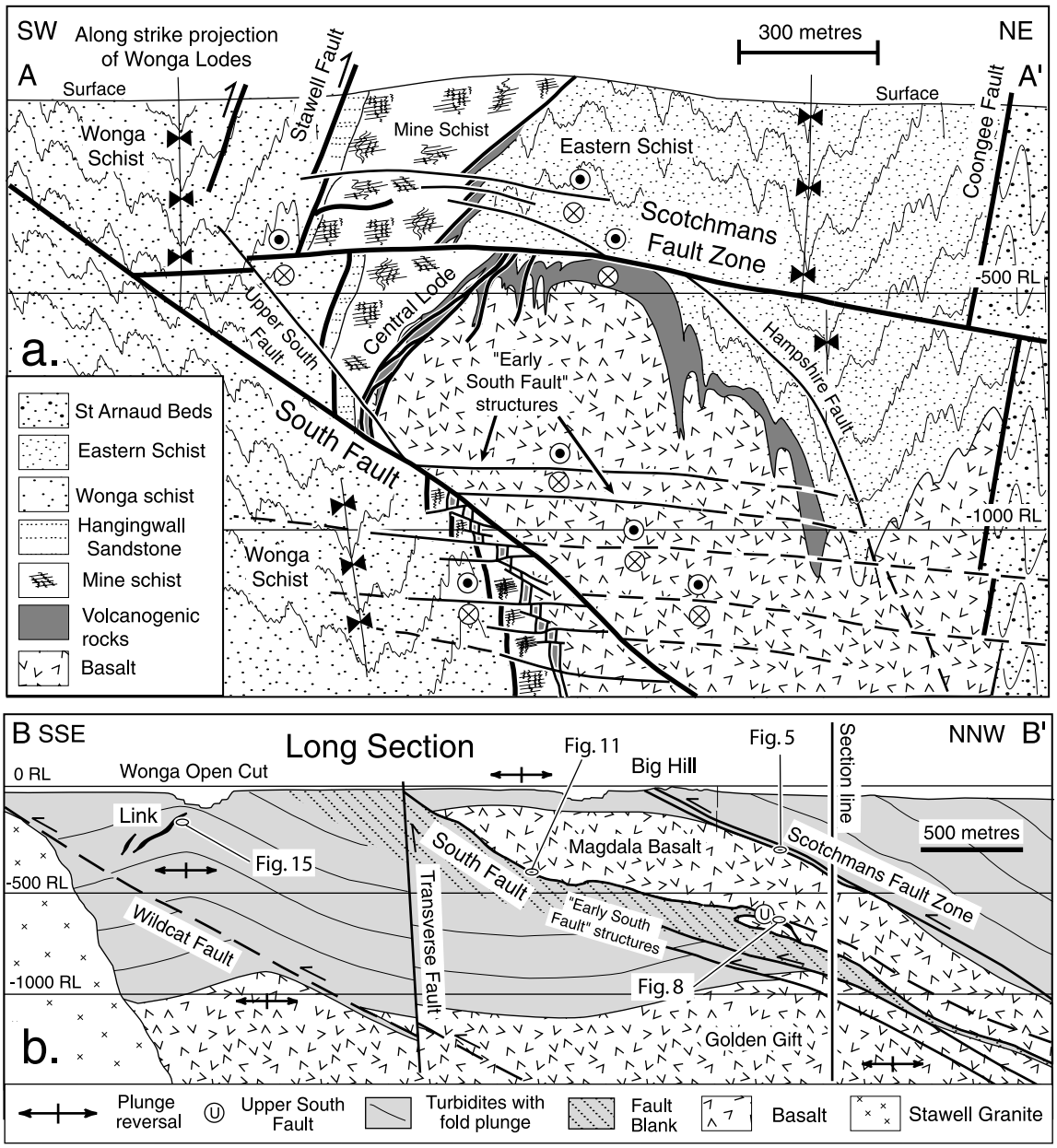

Fig. 2. Geological sections showing the mineralised zones at Stawell. (a) Cross-section of the Magdala System. (b) Long section through the Magdala and Wonga systems. Section lines are marked on Fig. 1c. The locations of Figs. 5, 8, 11 and 15 are also marked.

will produce normal and shear stresses favourable for reactivating each particular fault orientation.

Compression and tension dihedra were calculated where possible using the technique of Angelier (1984). The maximum principal palaeostress (σ_1) should lie somewhere in the white quadrants on the calculated dihedra, while the minimum principal palaeostress (σ_3) should lie in the grey quadrants (Fig. 3d). These principal stresses can, in some cases, be isolated by overlapping the dihedra for individual faults.

At several locations it was possible to calculate the net slip vector on a fault that showed clear evidence for a variable slip history by either: (1) utilising the offset of vein markers with different strikes across a fault on a drive wall; or (2) utilising three-dimensional trigonometry in areas where a fault intersected two planes containing clear marker horizons defining a measurable offset across the fault.

Stress inversion of fault slip data calculated from striations and extension veins was done using the program SLICK.BAS (Ramsay and Lisle, 2000). This predicts the orientations of the principal stresses, the stress shape ration (ϕ) and also evaluates the average angular deviation ($<°$) of the slip data with the theoretical predicted directions. The assumptions are: (1) that the slip direction on a fault is parallel to the resolved shear stress; (2) that slip data utilised reflects deformation within a homogeneous stress field; and (3) that there is independent slip (Ramsay and Lisle, 2000).

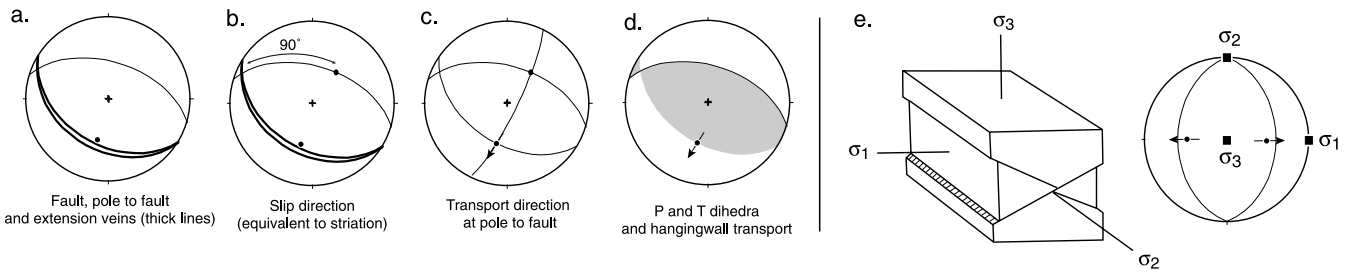

Fig. 3. (a)–(d) Stereographic projections demonstrating the calculation of hanging wall transport directions and also pressure and tension dihedra. The slip direction is perpendicular to the intersection of the extension veins with the great circle defining the fault ((a) and (b)). A great circle is drawn that contains the pole to the fault and the slip direction (c). The hanging wall transport direction is defined as an arrow drawn on the tangent to this second great circle at the point it intersects the pole to the fault ((c) and (d)). The arrow represents the transport direction of the rocks in the hanging wall of the fault. (e) Block model of conjugate faults (Andersonian geometry) and stereographic projection of inferred palaeostress fields and slip direction (hanging wall transport) associated with fault geometry. All stereonets are equal area.

Compressional stress has been depicted with a positive sign (cf. Ramsay and Lisle, 2000).

3. Regional setting

The Palaeozoic western Lachlan Fold Belt in south-eastern Australia is adjacent to the Grampians–Stavely Zone of the Delamerian Fold Belt (Gray, 1988; Fig. 1a). This region of the Lachlan Fold Belt is divided into three structural zones: the Stawell, Bendigo–Ballarat and Melbourne Zones. These are bounded by steep reverse faults and the turbidites are folded into tight upright folds (Fergusson et al., 1986; Cox et al., 1991; Wilson et al., 1992).

The Stawell Zone is sub-divided into two major structural regions by the steep west-dipping Coongee Break (Fig. 1a and b). To the west of this break the base of the local stratigraphy is comprised of massive and pillowed tholeiitic basalt conformably overlain by a sequence of rocks termed the 'Magdala volcanogenic rocks' (Watchorn and Wilson, 1989). These rocks are overlain by deformed sandstone and shale (Fig. 2a; Watchorn and Wilson, 1989). The dominant northwest-trending structural grain of the Stawell–Ararat Fault Zone is disrupted by a later system of northeast- to northwest-dipping faults (Fig. 1b and c). These northwest-dipping faults have regional extent and have deformed units within both the Lachlan and Delamerian Fold Belts (e.g. Silurian Grampians cover sequence; Fig. 1a).

The majority of the gold at Stawell (>5 million ounces) occurs on the western flank of the large, doubling-plunging, basalt dome (the Magdala Antiform; Fig. 2a and b). Gold lodes developed during brittle deformation associated with high fluid pressures in a northeast–southwest and then east–west shortening regime (Miller and Wilson, 2002a). These are termed the Magdala lodes and the recently discovered Golden Gift lodes (Watchorn and Wilson, 1989; Fredericksen and Gane, 1998; Dugdale and Fredericksen, 2000; Miller et al., 2001; Miller and Wilson, 2002a). The Golden Gift lodes represent an offset portion of the Magdala lodes (Fig. 2b; Dugdale and Fredericksen, 2000; Miller et al., 2001). Sericite separated from quartz veins sampled within the Magdala lodes produced a 439 Ma $^{40}Ar/^{39}Ar$ plateau age (Foster et al., 1998). Gold mineralisation is also associated with sinistral wrenching that overprints early brittle structures within the Magdala Mine (Miller and Wilson, 2002a).

The Magdala basalt dome and the gold lodes are dismembered by a later set of northwest-, north- and northeast-dipping faults (e.g. Scotchmans Fault Zone, the South Fault and the Upper South Fault; Fig. 2a and b). The smaller Wonga Deposit (~250,000 ounces Au) occurs within strongly foliated turbidites and is separated from the Magdala Deposit by the South Fault (Fig. 2b). This deposit occurs within the contact aureole of the Stawell pluton.

Quartz–feldspar porphyry dykes intrude parallel to existing structural weaknesses. U–Pb SHRIMP ages on zircons from a porphyry dyke at the Magdala Mine have an age of 413 ± 3 Ma (Arne et al., 1998). These dykes intrude mineralised Magdala lodes, but they are truncated and mineralised by the Wonga gold deposit. The Wonga lodes are contact metamorphosed by the early Devonian Stawell pluton (Wilson et al., 1999). This provides a tight age constraint for the Wonga Mineralisation of between 413 and 401 Ma—younger than the $^{40}Ar/^{39}Ar$ 439 Ma age from the Magdala lodes (Foster et al., 1998).

The Stawell Zone is intruded by Early Devonian granitoids (401 ± 4 Ma U–Pb SHRIMP zircon age on the Ararat granodiorite in Arne et al. (1998)). Miarolitic cavities and the contact metamorphic assemblages adjacent to the plutons indicate a depth of intrusion of less than 5 km (Bird, 1986; Xu et al., 1994). Some of these Devonian plutons have intruded parallel to these faults (Fig. 1a and b; Miller et al., 2001). The Devonian Stawell pluton is a composite intrusion comprising three mappable magmatic phases of diorite, granodiorite and granite/adamellite (Bird, 1986).

4. Structural analysis

4.1. Scotchmans Fault Zone

The Scotchmans Fault Zone system of faults is parallel to

the top of the Magdala dome along its northwestern margin (Fig. 2). The fault zone has a general northeast trend and dips about 30° to the northwest. However, faults within this fault zone have variable strikes (Fig. 4). The top of the Magdala dome consists of highly variable stratigraphy, which reflects the complex series of basalt 'noses' that define the top of the Magdala Antiform. Many of these units are highly foliated due to earlier ductile deformation of the system (Miller and Wilson, 2002a). The dip of the foliation is commonly parallel to the dip of the underlying basalt and may reflect ductile shearing parallel to the lithological contact between the Magdala volcanogenic rocks and the underlying basalt.

Mapping of synthetic faults in the footwall of Scotchmans Fault Zone highlights that these faults commonly have dips that are identical to the older foliation (compare the faults on section c–c′ on Fig. 5 to those on section line a–a′), and appear to have propagated along the variably oriented foliation and bedding surfaces (e.g. northeast-dipping faults highlighted on Fig. 4). The fault surfaces are commonly striated with the striation defined by either fault grooves or quartz fibres (Fig. 6a) and in some cases alteration minerals (sericite, chlorite, epidote) define a weak mineral lineation. Within the basalt and volcanogenic rocks these striations are commonly associated with southwest- and south-directed hanging wall transport (Figs. 5 and 7e). Striations on fault surfaces within Porphyry dykes in the hanging wall of the Scotchmans Fault Zone gave south- and north-directed hanging wall transport (Fig. 7c). Striae on graphitic fault surfaces in the direct footwall of the fault

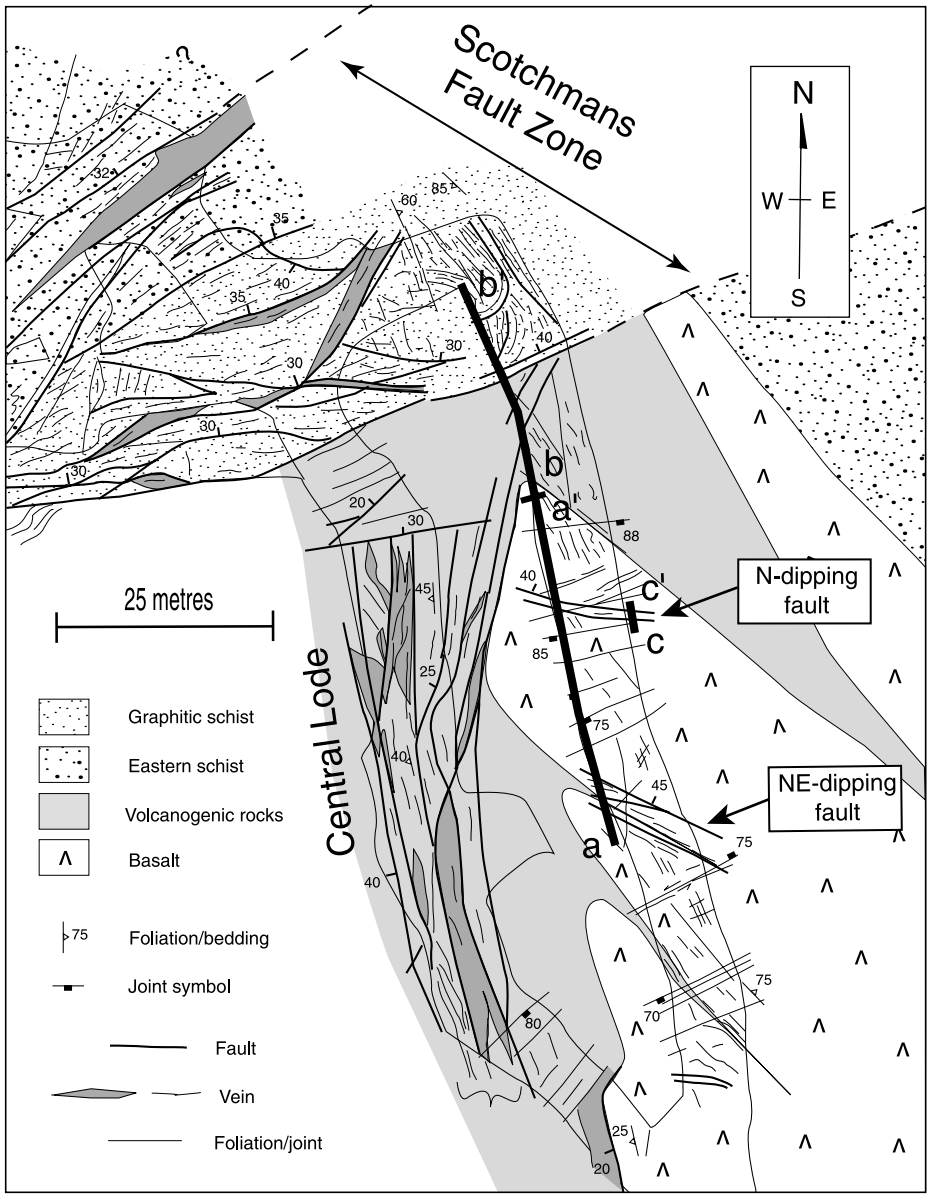

Fig. 4. Geological map of Scotchmans Fault Zone on the 290 RL. Section lines for Fig. 5 are marked. Map compiled from underground mapping and diamond drilling by mine geologists at Stawell.

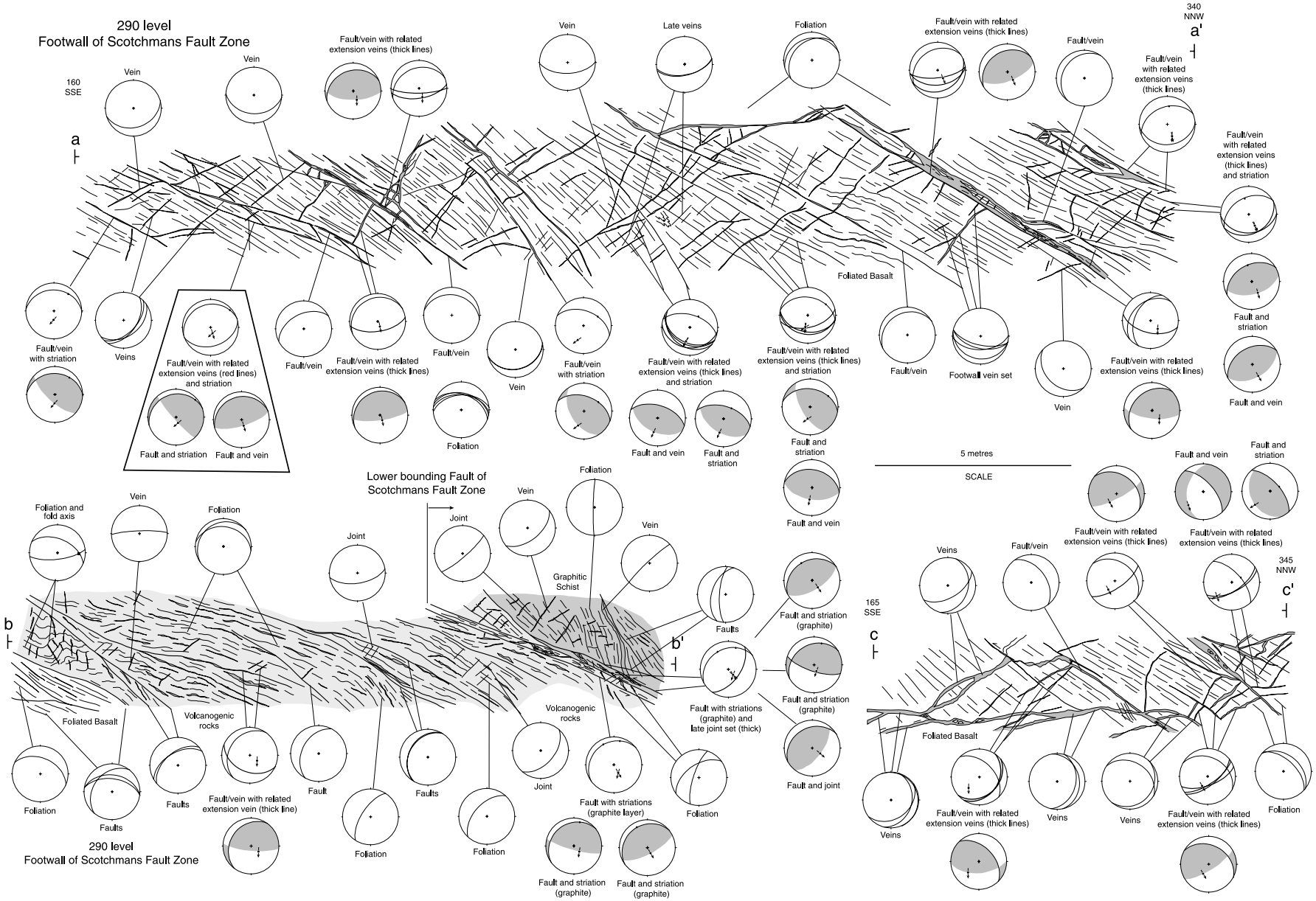

Fig. 5. Structural profiles in the direct footwall of Scotchmans Fault Zone on the 290 RL. Section lines are marked on Fig. 4. Faint lines depict cleavage traces or joints, thicker lines are veins or faults, grey infilled features are quartz veins. Stereonets are equal area.

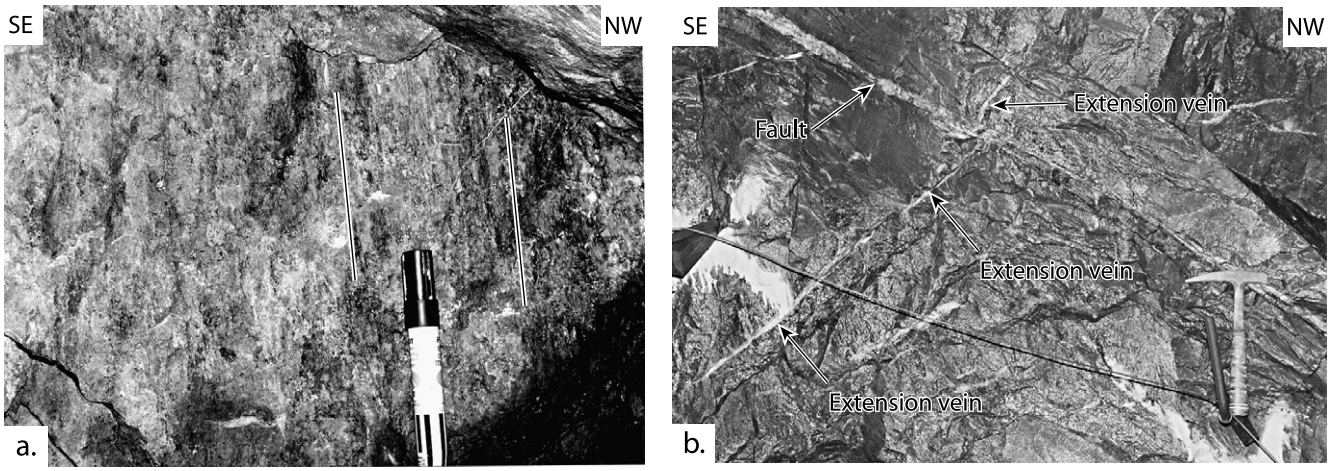

Fig. 6. Structural features within Scotchmans Fault Zone on the 290 RL. (a) Late striations defined by alteration minerals and wear grooves. Marker pen shown for scale. (b) Northwest-dipping fault and associated extension veins used to delineate hanging wall transport direction (Fig. 7). Geological hammer shown for scale.

zone indicate late southeast- and south-directed hanging wall transport (Fig. 7e).

In contrast to the striation data, the use of extension veins adjacent to the faults (Fig. 6b) to define hanging wall transport directions produced top-to-the-south and top-to-the-southeast directed transport (Figs. 5 and 7a). In many cases the southeast-directed transport occurred irrespective of the strike of the actual faults (Fig. 5). In some cases, distinctly different transport directions were recorded by striations and extension veins for the same fault (stereonets within the trapezium in Fig. 5). No gold was recognised associated with veining parallel to the faults or in footwall or hanging wall extension veins.

4.2. Upper South Fault (672 RL and 728 RL)

The Upper South Fault is a steep north-dipping fault at the base of the Magdala ore body (Fig. 2). Striations defined by quartz-fibres on the Upper South Fault have both flat and steep rakes (Figs. 8 and 9). The rocks defining the footwall of the Upper South Fault are distinct in that the dominant cleavage (S_2) dips steeply to the east (instead of the moderate to steep west-dipping foliation within the hanging wall). In some areas east–west trending folds occur where foliated shales define the footwall (Fig. 10a).

The Upper South Fault is associated with a series of shallowly north- to northeast-dipping faults within both the hanging wall and footwall (Figs. 8 and 10b). The timing relationship of these faults with respect to the steeply dipping Upper South Fault was not constrained. The orientation of the Upper South Fault is similar to the late transverse faults documented elsewhere (Section 4.4).

Striations on the shallowly-dipping fault surfaces comprise quartz slickenfibres (Fig. 10c) and wear grooves (Fig. 10d). The wear grooves commonly have hanging wall transport directions of top-to-the-southwest while the quartz-fibres are top-to-the-south (Fig. 9). Analysis of vein markers with distinctly different orientations across one of these faults allowed a net transport vector to be calculated and this corresponds with a net transport of top-to-the-south (Fig. 10e). The last stage of brittle deformation observed within the Upper South Fault block is defined by slip along foliation surfaces. These have pronounced striations defined by wear grooves that rake steeply to the southeast (Figs. 8 and 9).

4.3. South Fault (460 RL)

The South Fault is a major late fault at Stawell that delineates the base of the offset Magdala Basalt (Fig. 2a and b). The South Fault trends northwest–southeast and dips between 40 and 50° to the northeast (Miller et al., 2001). Minor late faults with similar orientations occur throughout the Magdala Mine. Veins related to these ‘South Fault-age’ structures are associated with calcite and quartz rather than quartz, which is the dominant vein type associated with earlier faults.

At the 460 level of the Magdala Mine the South Fault is a sharply defined break with minor fault gouge (Figs. 11 and 12). The hanging wall of the fault is defined by deformed volcanogenic rocks with S–C fabrics, giving a reverse movement sense (Figs. 11 and 12). The footwall of the fault contains a series of low-angle faults that splay off the South Fault. Porphyry dykes adjacent to the South Fault are clearly truncated and buckled by either the South Fault or related footwall splays (Fig. 12a). The footwall dykes contain extension veins (Fig. 12b) and the extension or stretching direction recorded by these veins in the footwall of the South Fault indicates dip-slip (reverse) movement on the South Fault (i.e. a hanging wall transport of top-to-the-southwest; Fig. 13). Graphitic layers on the actual South Fault surface have wear grooves indicative of late top-to-the-southeast transport (Fig. 13).

The direct hanging wall of the South Fault preserves

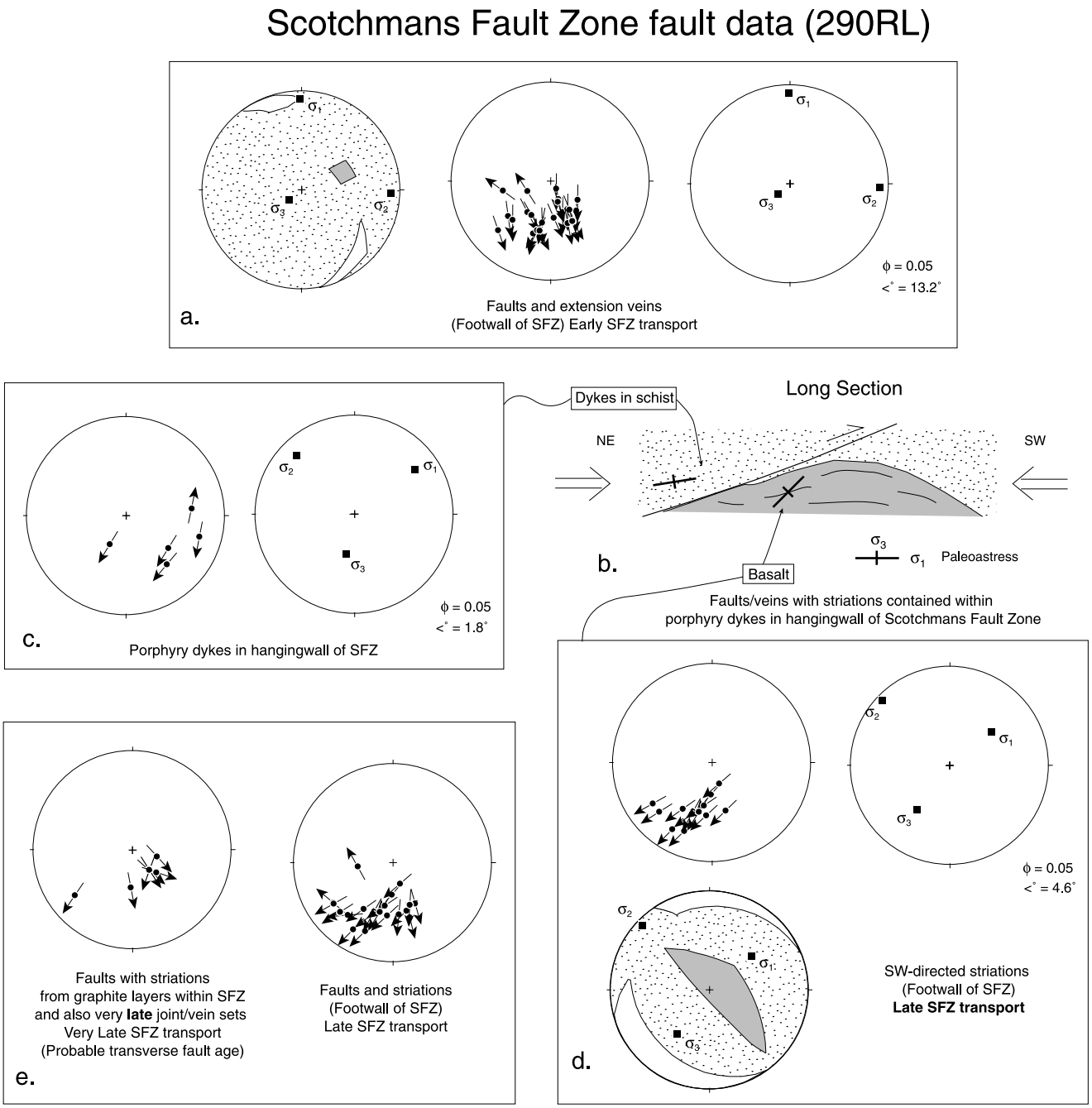

Fig. 7. Summary diagram of fault transport data from the Scotchmans Fault Zone region (290 RL). Palaeostress estimates were calculated using SLICK.BAS and also overlapping of compression and tension dihedra (white region corresponds to field containing σ_1, grey region corresponds to field containing σ_3). See text for discussion. Stereonets are equal area.

evidence of a complex structural history. Most of the veining is related to early regional brittle deformation associated with northeast–southwest shortening and later north–south-trending brittle faults with a component of sinistral offset (Miller et al., 2001; Fig. 11). All of these structures are overprinted by extensive shallowly (20 and 30°) dipping thrusts that have strikes ranging from northwest- to northeast-trending (Fig. 11). Hanging wall transports on these faults show two dominant directions (Figs. 11 and 13). Transport directions defined by the use of extension veins are dominantly top-to-the-southeast while transport directions defined by the use of striations are commonly top-to-the-southwest or top-to-the-south. Faults with transports of top-to-the-southwest overprint the faults with top-to-the-southeast transport (refer to annotation on Fig. 11). There are also extensive conjugate joint sets in the hanging wall of the South Fault. These joints dip to the northeast and southwest (Figs. 11 and 13).

In the hanging wall of the South Fault earlier veins and fault structures in the drive ceiling and walls in some places

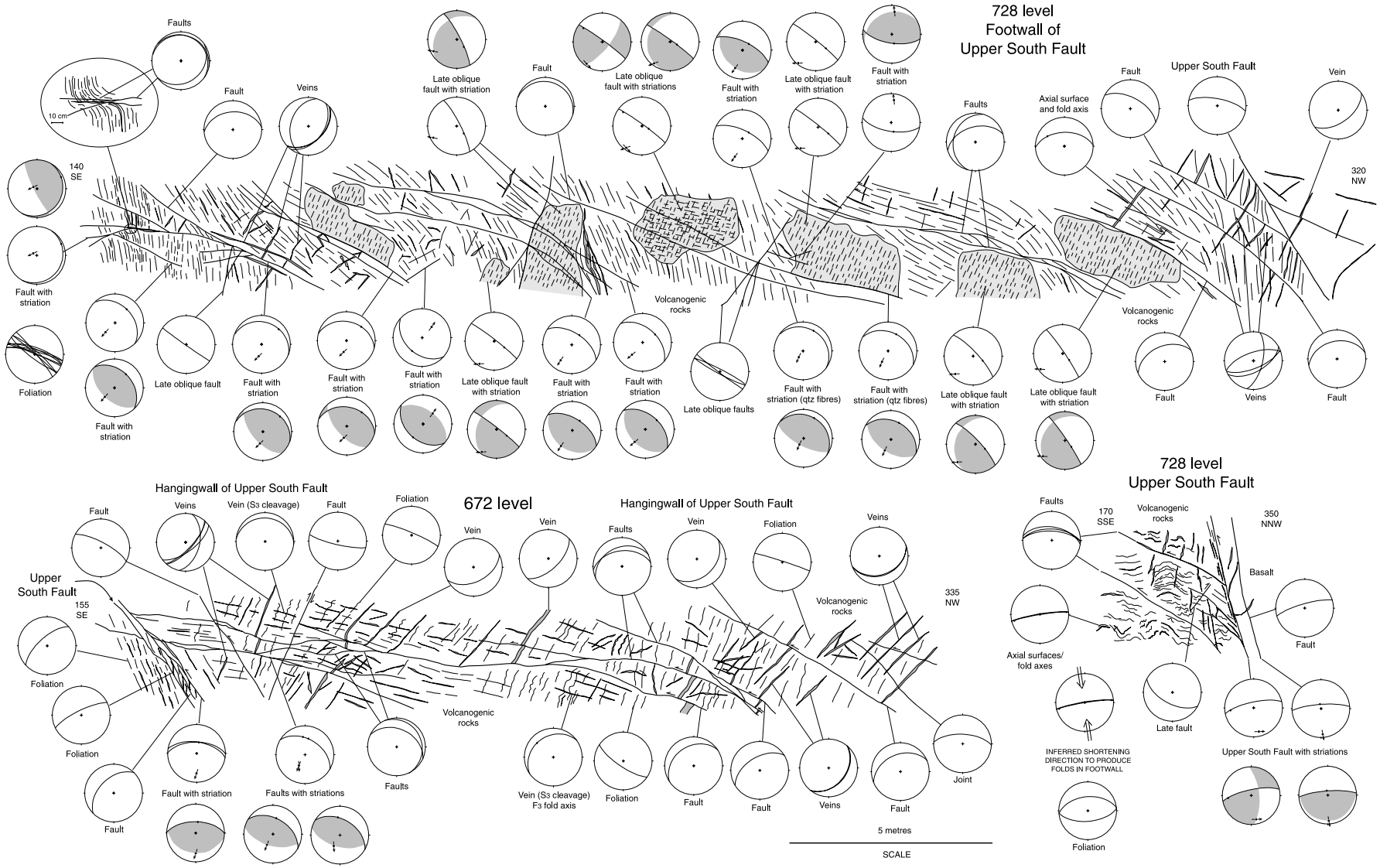

Fig. 8. Structural profiles of the Upper South Fault (728 RL, bottom right side of figure) and profiles through its direct footwall (728 RL) and hanging wall (672 RL). Approximate position of section lines are marked on Fig. 2b. Faint lines depict cleavage traces or joints, thicker lines are veins or faults, grey in-filled features are quartz veins. Stereonets are equal area.

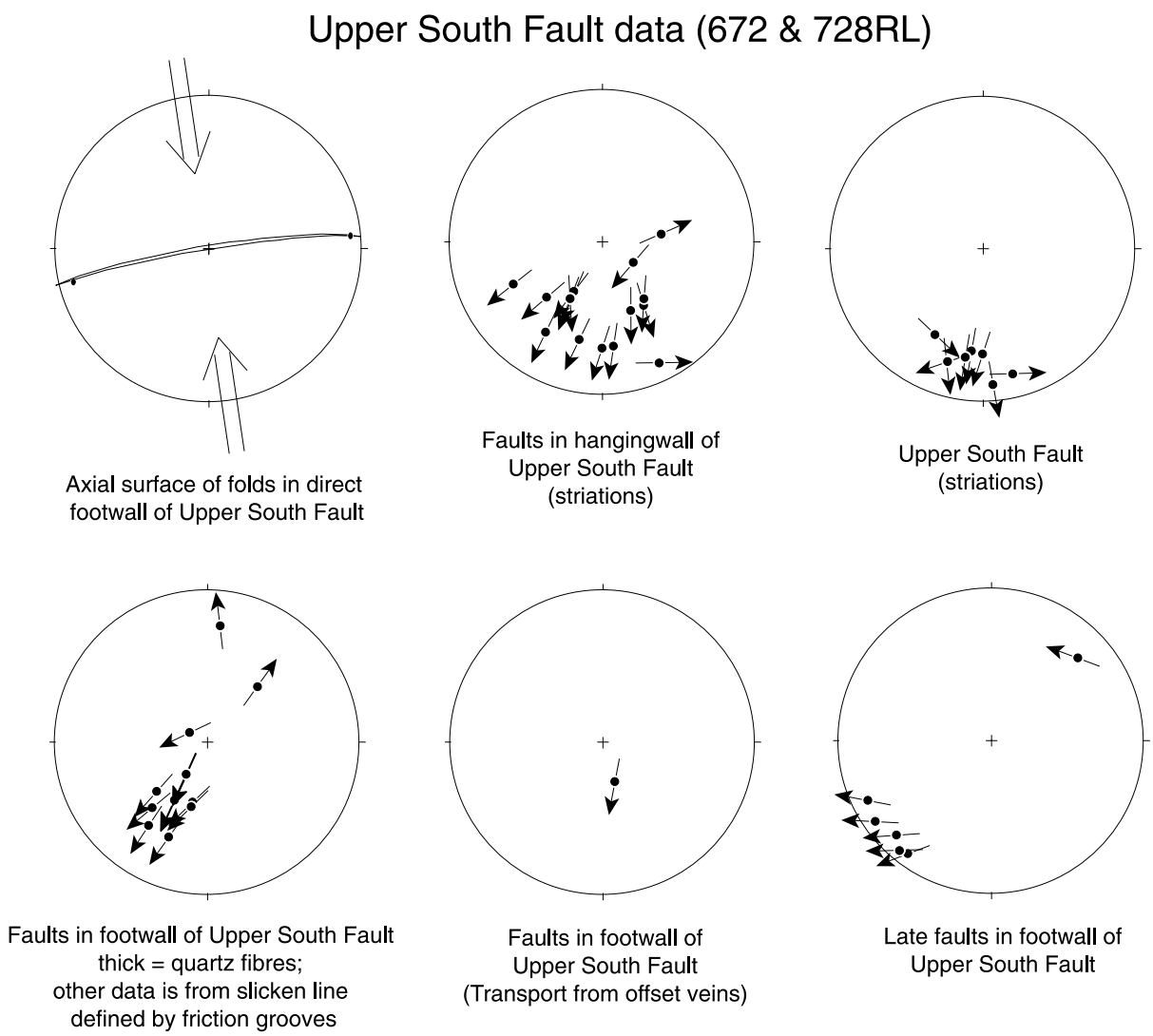

Fig. 9. Summary diagram of fault transport data from the Upper South Fault (672 and 728 RL). See text for discussion. Stereonets are equal area.

have measurable offset across the northwest-dipping faults. The ability to measure the offsets of more than one element on surfaces with different orientations allowed a net hanging wall transport direction towards 150° to be calculated via trigonometry (Miller et al., 2001; Fig. 11).

4.4. Wonga Mine

Brittle structures within the Wonga Mine reflect footwall deformation beneath the structures defining the South Fault system (Fig. 2b). The Wonga Mine has a similar deformation history to the Magdala deposit (i.e. early S_1 to S_3 cleavages and later reverse faults; Wilson et al., 1999; Miller and Wilson, 2002b). All of these features are crosscut by porphyry dykes. Unlike the Magdala deposit, brittle deformation associated with the Wonga Gold Lodes also affects the porphyry dykes (Wilson et al., 1999). Furthermore the mineralised vein structures at Wonga are not laminated (like the Magdala deposit) but are generally massive with angular clasts of wall rock in the veins. The Wonga deposit also contains markedly different mineralogy compared with the Magdala Lodes. The mineralogy is indicative of a magmatic association with mineralisation—acicular arsenopyrite, stibnite, gold telluride alloys, bismuth, silver and late stage molybdenite. Sulphur isotopes from arsenopyrite in the Wonga-style lodes have magmatic values and are isotopically distinct to the euhedral arsenopyrite within the Magdala deposit (Andrew et al., 2002).

Overall the Wonga system consists of two main lode types (Fig. 14), these being the northwest-dipping hanging wall structures and southeast-dipping links (or splays). The links commonly have an en-échelon geometry with the hanging wall structures and the style of mineralisation is one of localised failure that does not occur within one master shear zone. The hanging wall structures either localise along the northeast-dipping S_3 cleavage or adjacent to the boundary between the northeast-dipping porphyry dykes and the Wonga Schist wallrock. Kinematic analysis of the hanging wall structures indicates the Wonga lodes have a

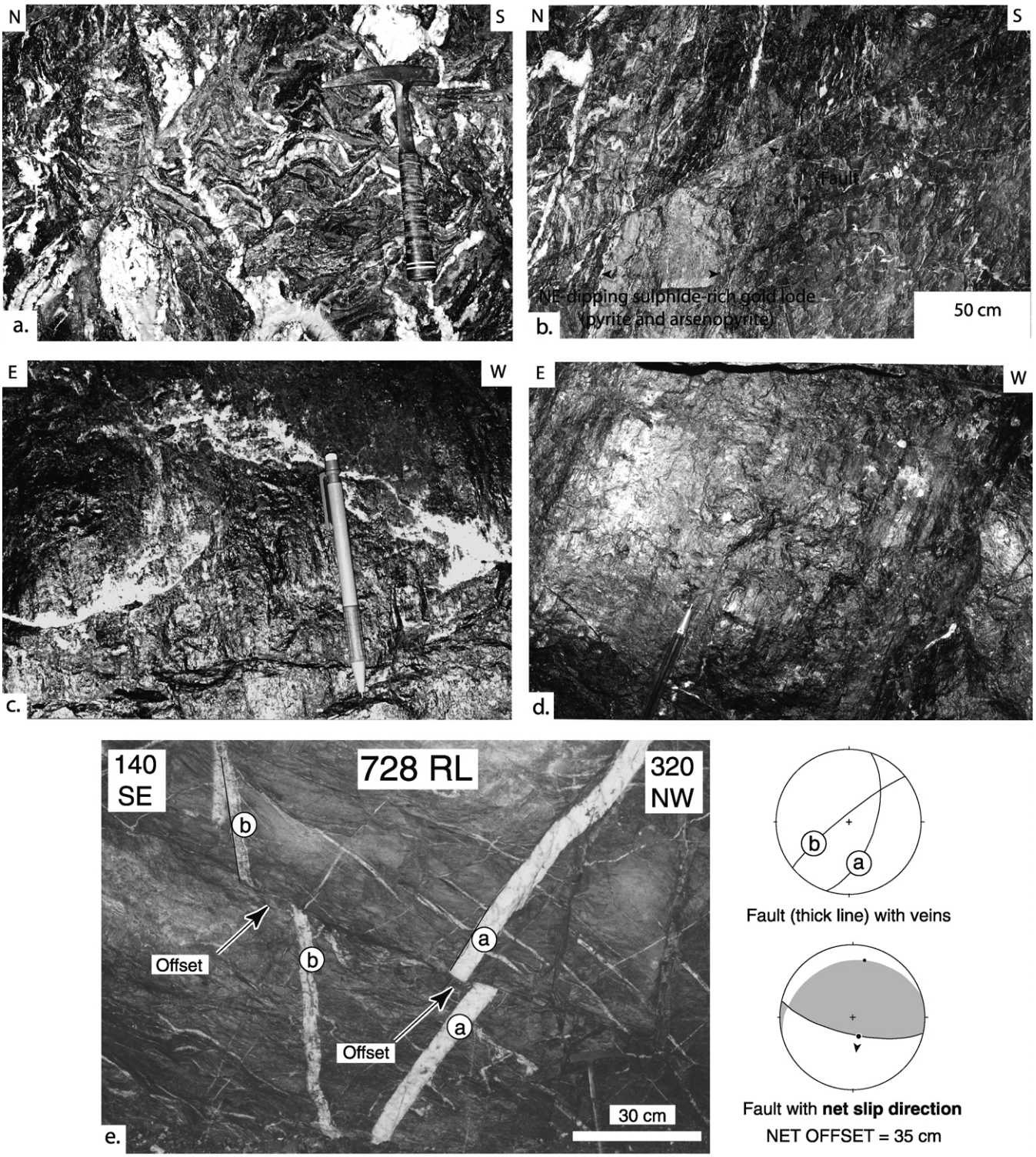

Fig. 10. Structural features near the Upper South Fault. (a) Folds within the direct footwall of the Upper South Fault (728 RL). These folds are documented on Fig. 8. (b) Shallowly north-dipping fault in the direct footwall of the Upper South Fault. Note truncation of gold ore in the footwall of this fault. (c) Striations on a north-dipping fault defined by quartz fibres—this is the same fault surface as (d). Pencil shown for scale. (d) Late striations on a north-dipping fault defined by wear grooves—this is the same fault surface as (c). Pen shown for scale. (e) Underground photograph of veins with different orientations offset across northwest-dipping fault in the footwall of the Upper South Fault (728 RL). Note the different amounts of apparent offsets. Right-hand side of diagram highlights calculation of net slip using the projected intersection of the intersection between the two veins as a marker. Hammer shown for scale.

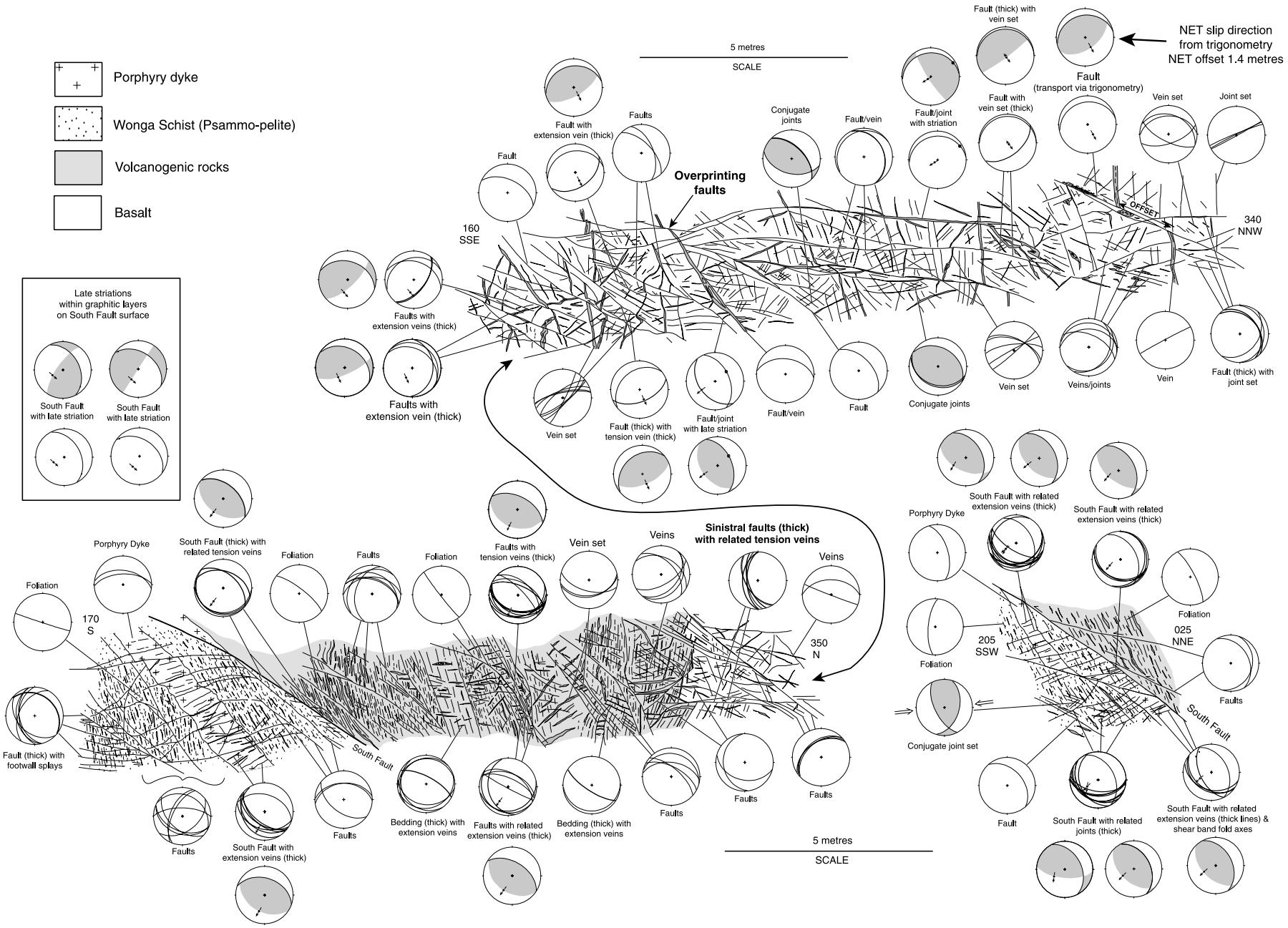
Porphyry dyke
Wonga Schist (Psammo-pelite)
Volcanogenic rocks
Basalt
Late striations within graphitic layers on South Fault surface
South Fault with late striation
South Fault with late striation
5 metres
SCALE
Fault with extension vein (thick)
Faults
Fault
Overprinting faults
160 SSE
Conjugate joints
Fault/vein
Fault/joint with striation
Fault (thick) with vein set
Fault with vein set (thick)
Fault (transport via trigonometry)
NET slip direction from trigonometry
NET offset 1.4 metres
Vein set
Joint set
OFFSET
340 NNW
Faults with extension veins (thick)
Faults with extension vein (thick)
Vein set
Fault (thick) with tension vein (thick)
Fault/joint with late striation
Fault/vein
Fault
Conjugate joints
Vein set
Veins/joints
Vein
Fault (thick) with joint set
Porphyry Dyke
South Fault (thick) with related tension veins
Foliation
Faults
Foliation
Faults with tension veins (thick)
Vein set
Veins
Sinistral faults (thick) with related tension veins
Veins
170 S
350 N
Fault (thick) with footwall splays
South Fault
Faults
South Fault with extension veins (thick)
Faults
Bedding (thick) with extension veins
Faults with related extension veins (thick)
Bedding (thick) with extension veins
Faults
Faults
Faults
5 metres
SCALE
South Fault with related extension veins (thick)
South Fault with related extension veins (thick)
Porphyry Dyke
Foliation
205 SSW
Foliation
025 NNE
Faults
Conjugate joint set
South Fault
Fault
South Fault with related joints (thick)
South Fault with related extension veins (thick lines) & shear band fold axes

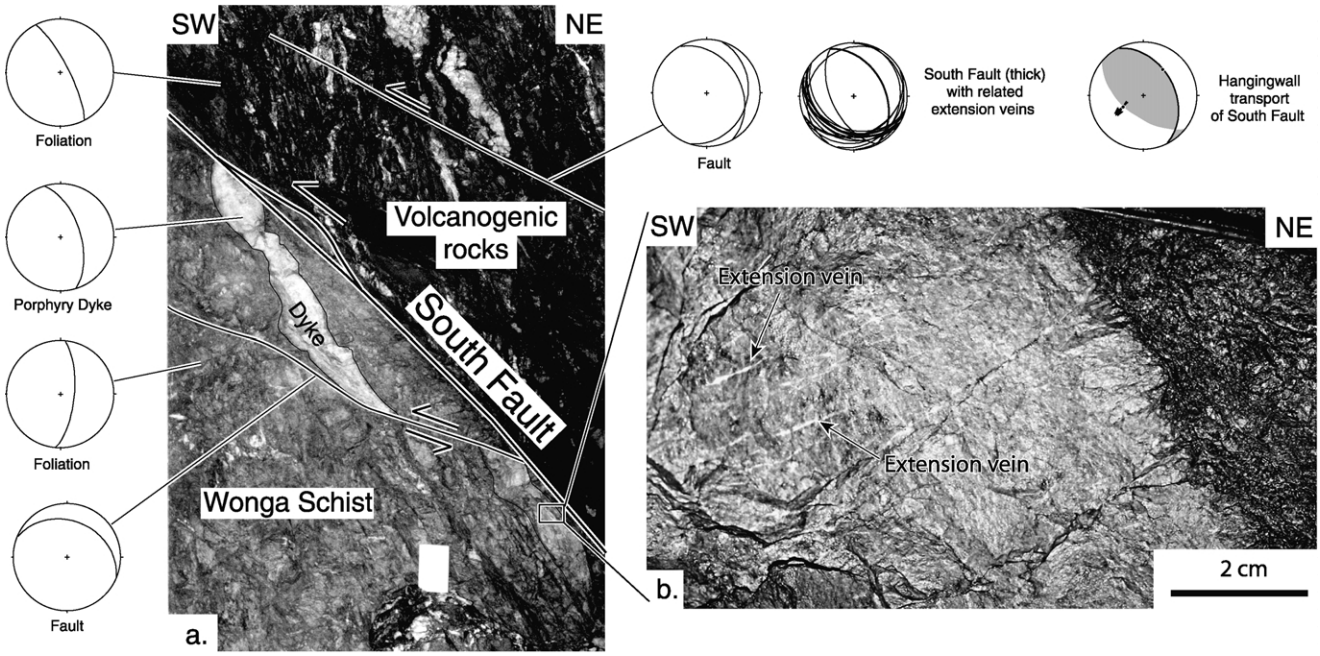

Fig. 12. Annotated photographs of the South Fault with structural and kinematic data (460 RL). (a) South Fault. Note truncation of porphyry dykes and steep northeast-dipping foliation within the hanging wall. Notebook shown for scale. Modified from Miller et al. (2001). (b) Extension veins in a porphyry dyke in direct footwall of South Fault.

top-to-the-south or top-to-the-south–southwest hanging wall palaeotransport (Figs. 14 and 15) and are oblique-slip structures with a dextral component. This may be due to failure along pre-existing weaknesses (S_3 cleavage and porphyry dykes). The Wonga lodes overprint a northeast- to east-striking crenulation cleavage (Fig. 16a) that is oblique to earlier foliations (i.e. S_1 to S_3).

Within the Wonga Mine small synthetic faults of an inferred South Fault age also occur (Figs. 14, 15 and 16b). Striations, footwall vein sets and joints indicate a top-to-the-southwest movement sense for these structures (Fig. 14). These faults are associated with marked sericite, carbonate and pyrite alteration (Fig. 16b) that overprints the contact metamorphism associated with the Stawell pluton (granodiorite phase) and have been documented by Wilson et al. (1999).

Later faults termed the 'Transverse faults' strike east–west and overprint the earlier northwest–southeast striking faults with extensive hydrothermal alteration (Figs. 14–16). These faults are very planar features and dip steeply to the north. They are reverse faults with a component of dextral offset (Fig. 15) and have regional extent (Fig. 2b). The final stage of brittle structures documented are a set of north–south striking reverse faults that dip steeply both east and west (Fig. 14).

4.5. Porphyry dykes

The porphyry dykes provide a key timing relationship as they intrude parallel to some of the northwest-dipping faults that dismember the Magdala Dome (Miller et al., 2001). Documented deformation within the porphyry dykes is as follows: (1) south-directed hanging wall transport associated with dextral oblique slip within the Wonga Mine (Fig. 14); (2) south-directed hanging wall transport above the Scotchmans Fault Zone (Fig. 7c); and (3) southwest-directed transport associated with the South Fault (Figs. 12 and 13). In no locality was southeast-directed transport observed overprinting these dykes. The orientation of the porphyry dykes is highly variable (Fig. 16d–g). The great circle fitted to a plot of poles to these dykes has a pole that plunges gently to the northwest (Fig. 16d).

5. Discussion

5.1. Overprinting criteria, fault transport data and palaeostress analysis

Underground mapping has previously demonstrated that the northwest- and north-dipping faults offset the Magdala

Fig. 11. Structural profiles of the South Fault and also its hanging wall (460 RL). Approximate position of section lines is marked on Fig. 2b. Faint lines depict cleavage traces or joints, thicker lines are veins or faults, grey in-filled features are quartz veins. Stereonets are equal area. Modified from Miller et al. (2001).

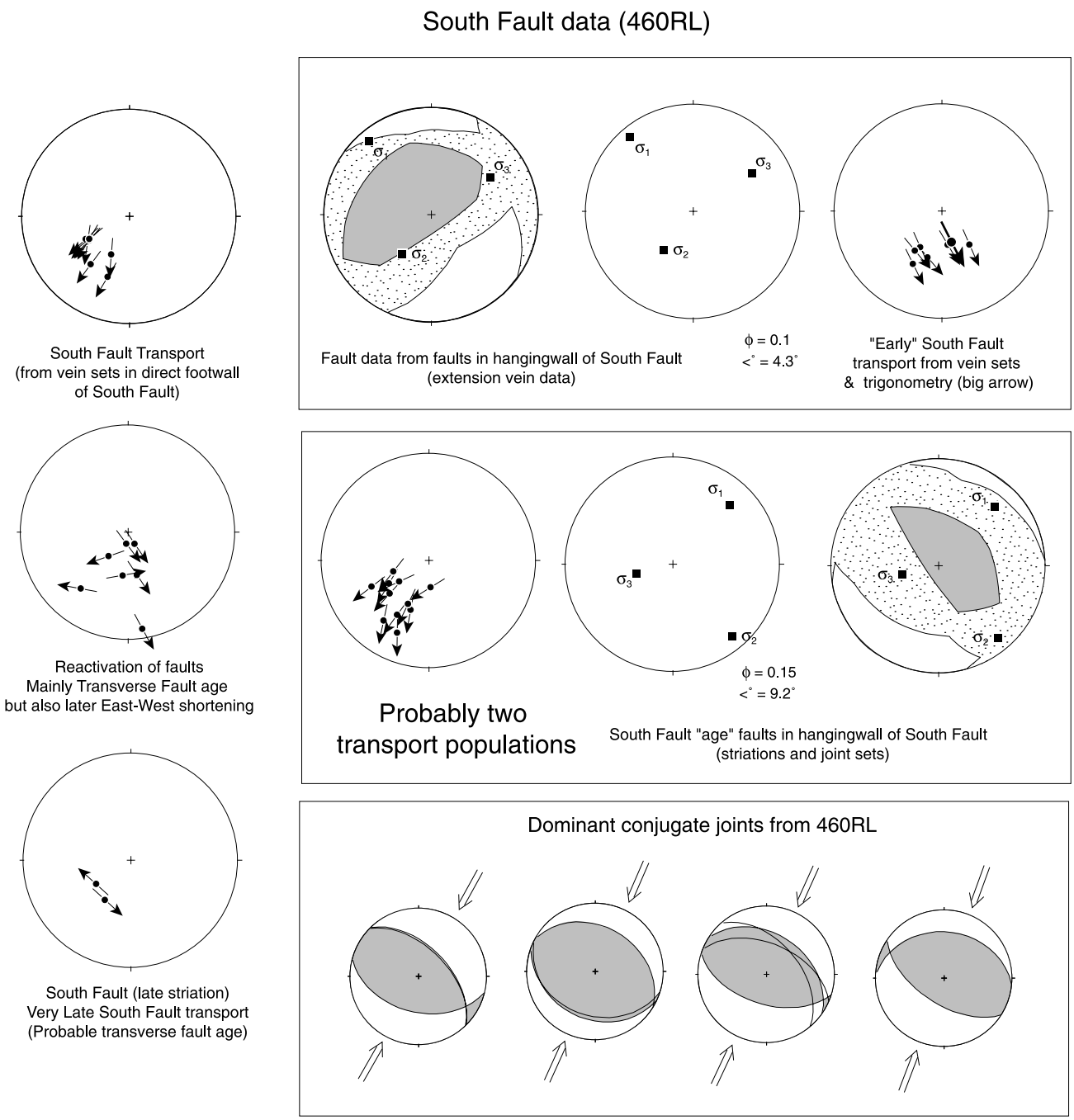

Fig. 13. Summary diagram of fault transport data from the South Fault (460 RL). Palaeostress estimates were calculated using SLICK.BAS and also overlapping of compression and tension dihedra (white region corresponds to field containing σ_1, grey region corresponds to field containing σ_3). See text for discussion. Stereonets are equal area.

mesothermal gold lodes and also faults associated with sinistral wrenching (Miller et al., 2001). Use of footwall and hanging wall extension veins associated with these later faults produced both south- and southeast-direct hanging wall transport directions. In contrast, the use of striations (in many cases on the same faults; Fig. 5) produced a dominant hanging wall transport of top-to-the-southwest or -south. The fact that a single fault preserves evidence for different transport directions from footwall extension veins and striations is strong evidence for a change in stress tensor. This inference is also supported by the relationships with intrusive bodies. The southeast-transport is not present within the porphyry dykes while the southwest-directed transport clearly overprints these dykes (Figs. 12a and 16f) and the contact metamorphism associated with the Stawell granodiorite (Fig. 16b).

The ability to calculate a net transport vector at some localities that matched the transport direction calculated from

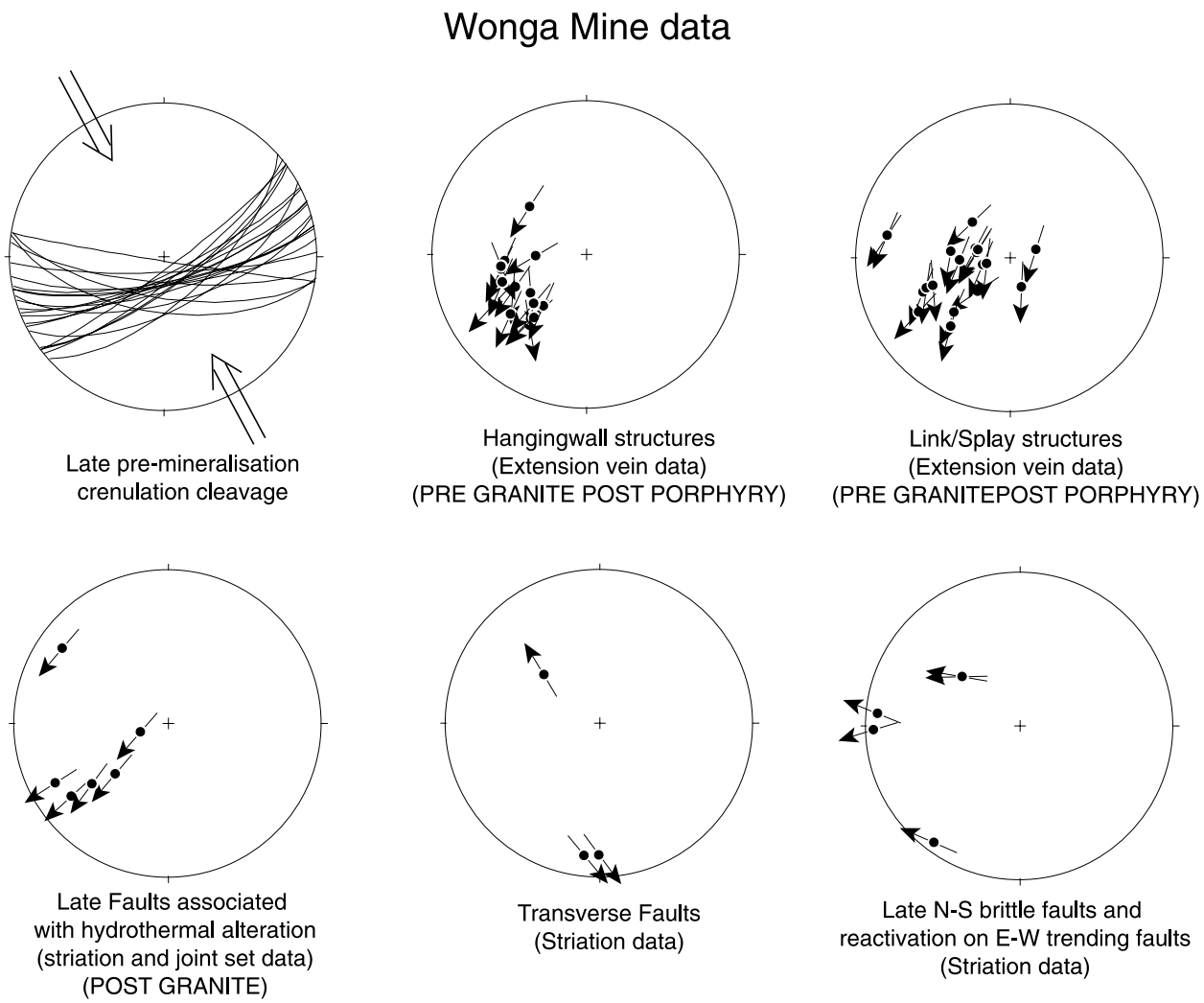

Fig. 14. Summary diagram of late crenulation cleavages and fault transport data from the Wonga Mine. See text for discussion. Stereonets are equal area.

footwall extension veins suggests that the use of extension veins to calculate transport directions is valid (e.g. Fig. 11). In the case of the Golden Gift discovery the use of footwall extension veins to define the potential direction in which the orebody lay was critical. If the striations on the fault surfaces had solely been used, the offset of the Magdala ore body would not have been correctly ascertained.

5.2. Southeast-directed transport and porphyry dykes

The input of fault-slip data calculated from footwall extension veins into SLICK.BAS for the Scotchmans Fault Zone (290 RL) and the South Fault (460 RL) localities produced two results—both with σ_1 flat-lying and oriented either northwest–southeast or north–south and values of ϕ between 0.05 and 0.15 (Figs. 7 and 13). The use of overlapping compression and tension dihedra calculated from footwall extension vein measurements produced possible fields of σ_1 and σ_3 consistent with both stress tensors produced with SLICK.BAS (Figs. 7 and 13). In summary the use of compression and tension dihedra combined with stress inversion of the slip data indicates σ_1 must have had a flat-lying orientation somewhere between the northwest and the north.

We will now compare the results of the stress inversion with the diagrams of theoretical resolved shear stress (Figs. 17–19). For a northwest-dipping fault theoretical resolved shear stress calculations produced both south- and southeast-directed transport if the σ_1 axis was flat-lying and in a north–south orientation (Fig. 18). However, southeast-directed transport will not occur on northeast-dipping faults in this stress regime (compare Fig. 17 with Fig. 18). The stress inversion for the Scotchmans Fault Zone data (290 RL) produced a north–south σ_1 as a valid solution (Fig. 7a). This palaeostress direction is not consistent with the southeast-directed hanging wall transport data on northeast-dipping faults from the 460 RL (and some faults on the 290 RL), that can only be produced if the σ_1 axis was flat-lying and in a northwest-southeast orientation (Fig. 17). Furthermore, on the 290 RL two transport directions calculated from extension veins occurred for faults with identical orientations. This implies that the slip data derived

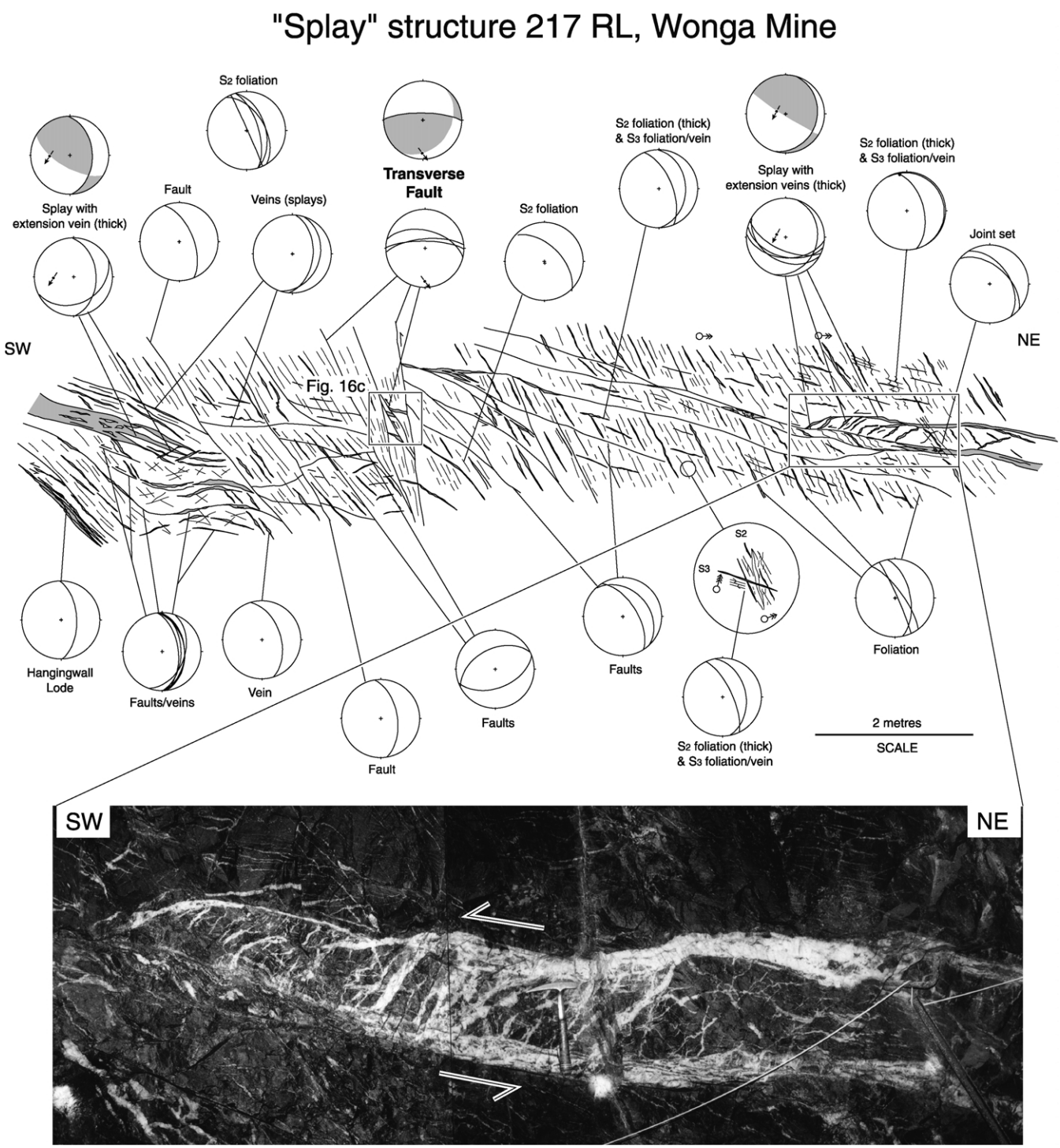

Fig. 15. Structural profile and photograph of a splay structure on the 217 RL of the Wonga Mine. Note the structure is offset by later east- to northeast-dipping faults and east–west oriented 'transverse faults'. Faint lines depict cleavage traces or joints, thicker lines are veins or faults, grey in-filled features are quartz veins. Stereonets are equal area. Approximate position of section line is marked on Fig. 2b. Location of Fig. 16c is also marked.

from extension veins represents more than one stress tensor. This appears to be reflected by the higher average angular deviation for the data from the 290 RL compared with that from the 460 RL (Figs. 7 and 13). A comparison of the diagrams of theoretical resolved shear stress indicates that all transport directions observed on the 290 RL could be related to a stress tensor in which σ_1 was flat-lying and oriented northwest–southeast with changes in σ_2 creating a variation in hanging wall transport direction producing some top-to-the-south directed transport (Fig. 17).

The porphyry dykes provide additional data on the possible palaeostress tensors. Field data has ascertained that

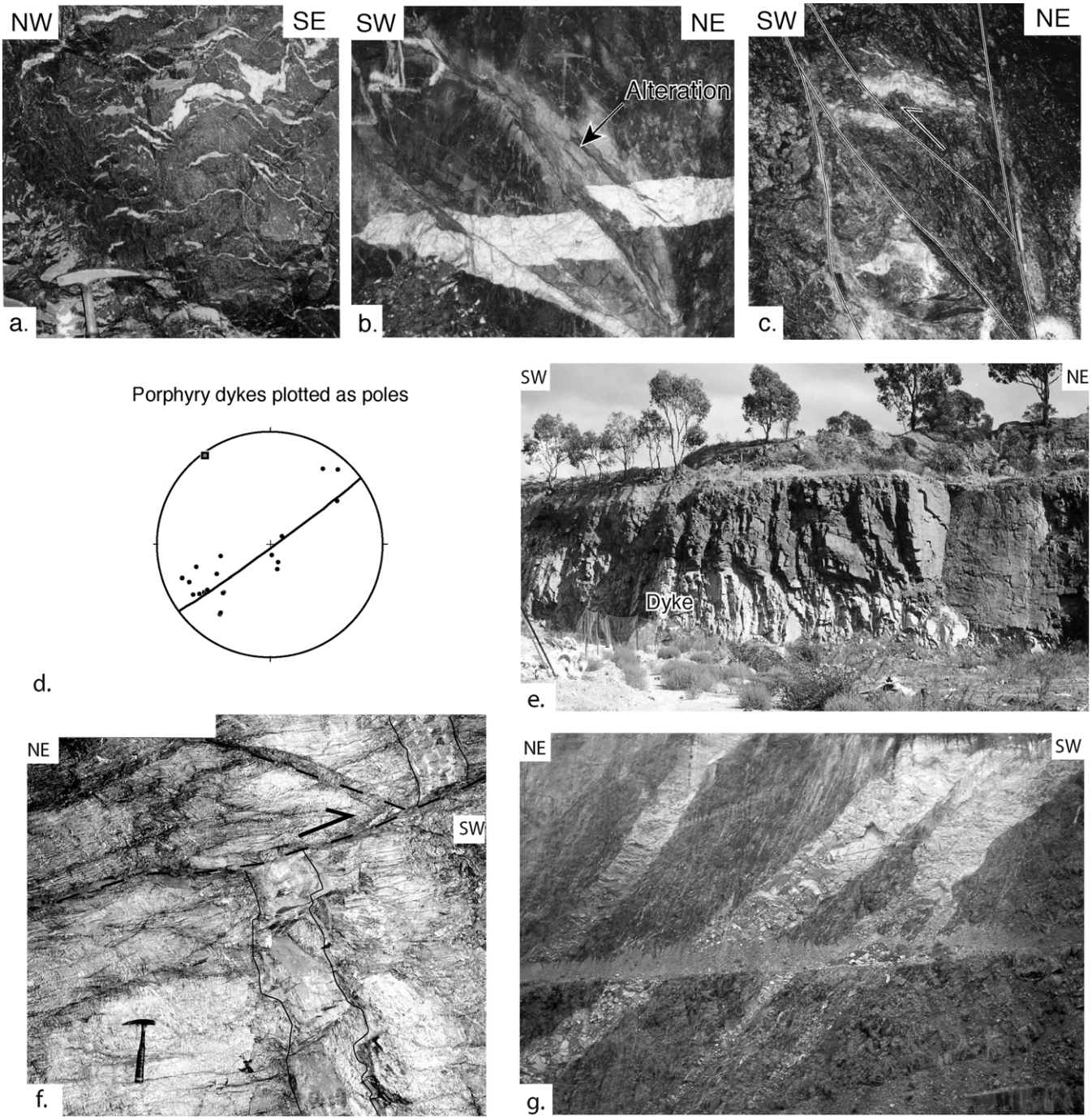

Fig. 16. Key structural features of the pre- and post-mineralised faults at the Wonga Mine. (a) Folds associated with late oblique crenulation cleavage. Geological hammer shown for scale. (b) Late northeast-dipping faults on the 307 RL associated with hydrothermal alteration that overprints contact metamorphism related to the intrusion of the Stawell pluton. Geological hammer shown for scale. (c) Late east–west-trending transverse faults on the −217 RL. Field of view is about 80 cm. Location of photo is marked on Fig. 20. (d) Equal area stereonet of poles to porphyry dykes within the direct vicinity of the Magdala and Wonga mines. (e) Northwest-dipping dykes within disused quarry. (f) Southwest-dipping dyke on the 90 RL, Magdala Mine. Dyke is offset by 'South Fault age' structure. Geological hammer shown for scale. (g) Northeast-dipping dykes within the Wonga open cut. Field of view approximately 50 m.

these dykes are not overprinted by southeast-directed transport and have intruded along the faults associated with southeast-directed transport after a significant component of transport had occurred (Miller et al., 2001). The opening direction of a dyke (and also an extension vein) generally corresponds to the local direction of minimum principal stress (σ_3). On a stereographic projection the orientation of σ_3 corresponds to the pole of the plane representing the dyke (or vein). In the case of the porphyries at Stawell there is not a consistent opening direction (Fig. 16d), which implies there is not a unique orientation of σ_3. This suggests that the dykes may have been associated with

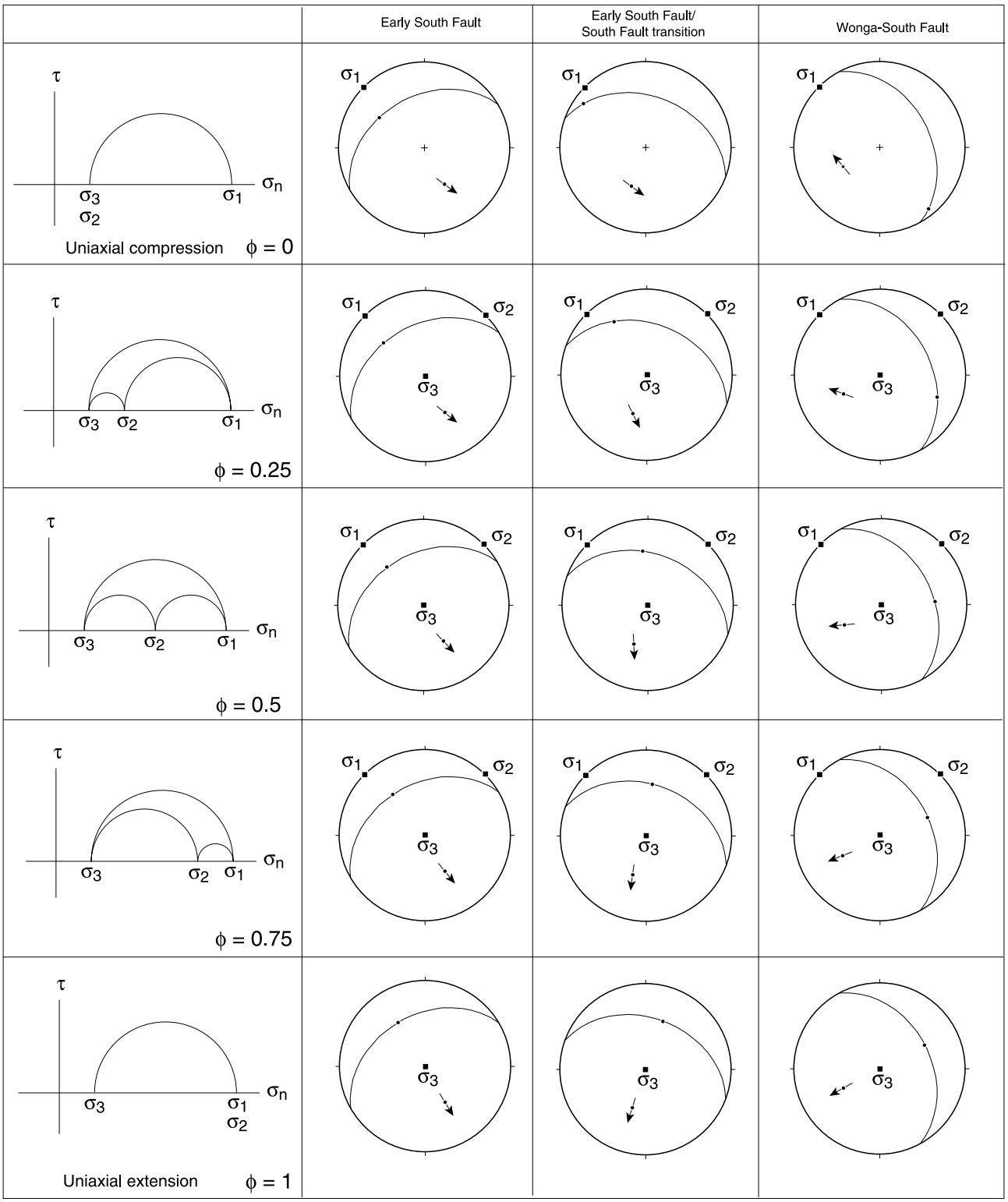

Fig. 17. Calculations of theoretical resolved shear stress for σ_1 with a flat-lying axis oriented northwest–southeast and σ_3 vertical.

a stress field in which there was no dominant σ_3 control i.e. $\sigma_2 \approx \sigma_3$ (or uniaxial compression). In the case of uniaxial compression the pole to a great circle fitted through poles to the dykes will give the orientation of σ_1. In the case of the Stawell data, this indicates σ_1 was flat-lying and oriented northwest–southeast (Fig. 20c)—identical to the inferred σ_1 direction for the faults associated with southeast- and south-directed transport.

A stress history consistent with the observed field relationships is that the initial stages of faulting associated

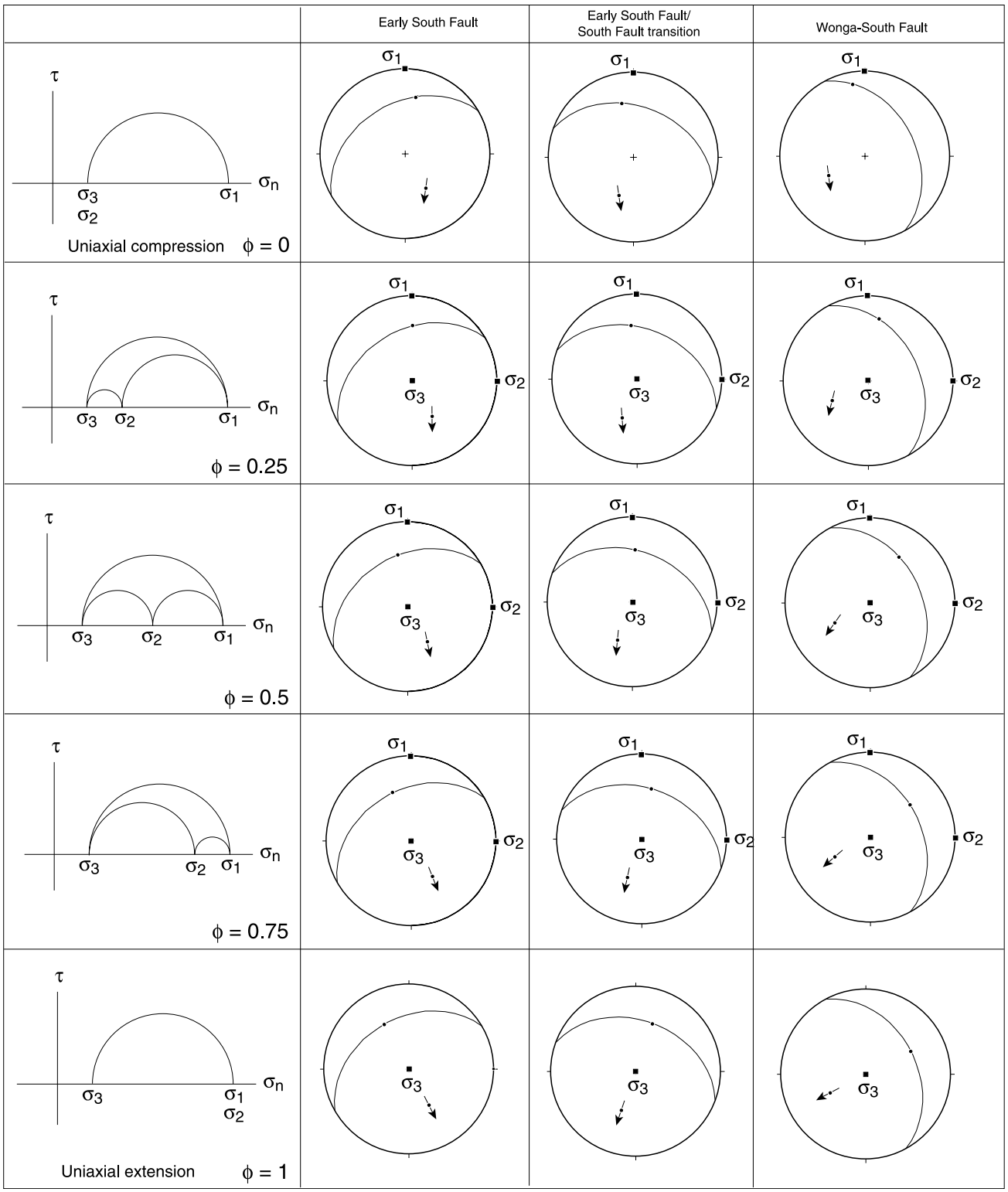

Fig. 18. Calculations of theoretical resolved shear stress for σ_1 with a flat-lying axis oriented north–south and σ_3 vertical.

with Scotchmans Fault Zone and the South Fault system of faults was related to a palaeostress field with σ_1 flat-lying and oriented northwest–southeast, σ_3 vertical and σ_2 larger than σ_3 producing both top-to-the-south and southeast-transport (e.g. $\phi \sim 0.5$; Fig. 20a). There was a gradual reduction in σ_2 initially producing dominant southeast-directed transport on all faults (Fig. 20b; $\phi \sim 0.25$) followed by dyke emplacement in the same stress field at the end stage or post the slip on the faults (Fig. 20c; $\phi \rightarrow 0.00$).

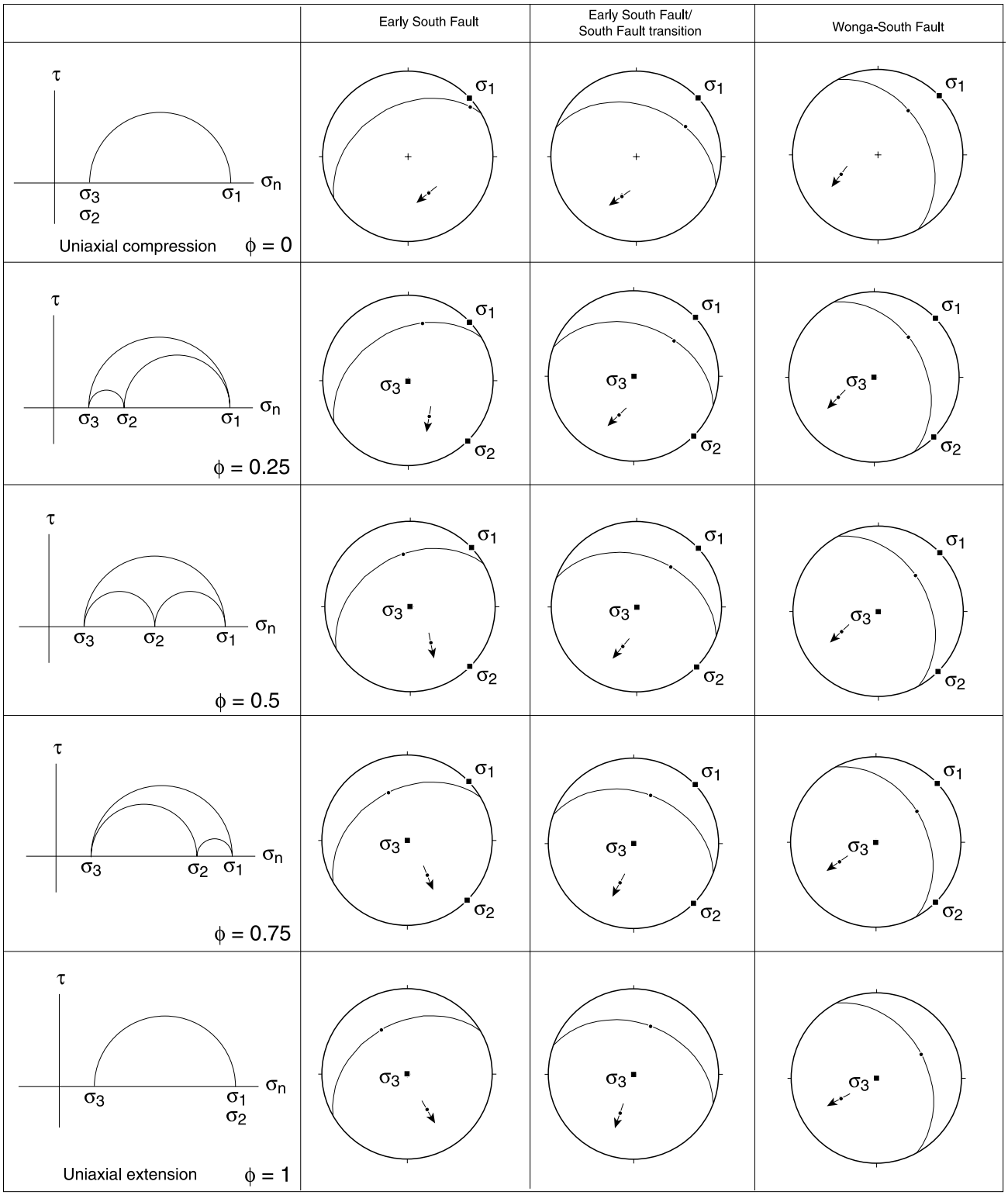

Fig. 19. Calculations of theoretical resolved shear stress for σ_1 with a flat-lying axis oriented northeast–southwest and σ_3 vertical.

If the above model for stress inversion is correct it implies the southeast-directed transport on the northwest-dipping faults represents movement associated with more than one stress tensor (i.e. $\phi = 0.00$ to $\phi = 0.5$). This means that care needs to be taken when subdividing slip data into independent subsets for use in stress inversion (either manually or via stress modelling software). The slip data from the northwest-dipping faults needs to be included in more than one subset.

One cannot rule out that some of the south-directed

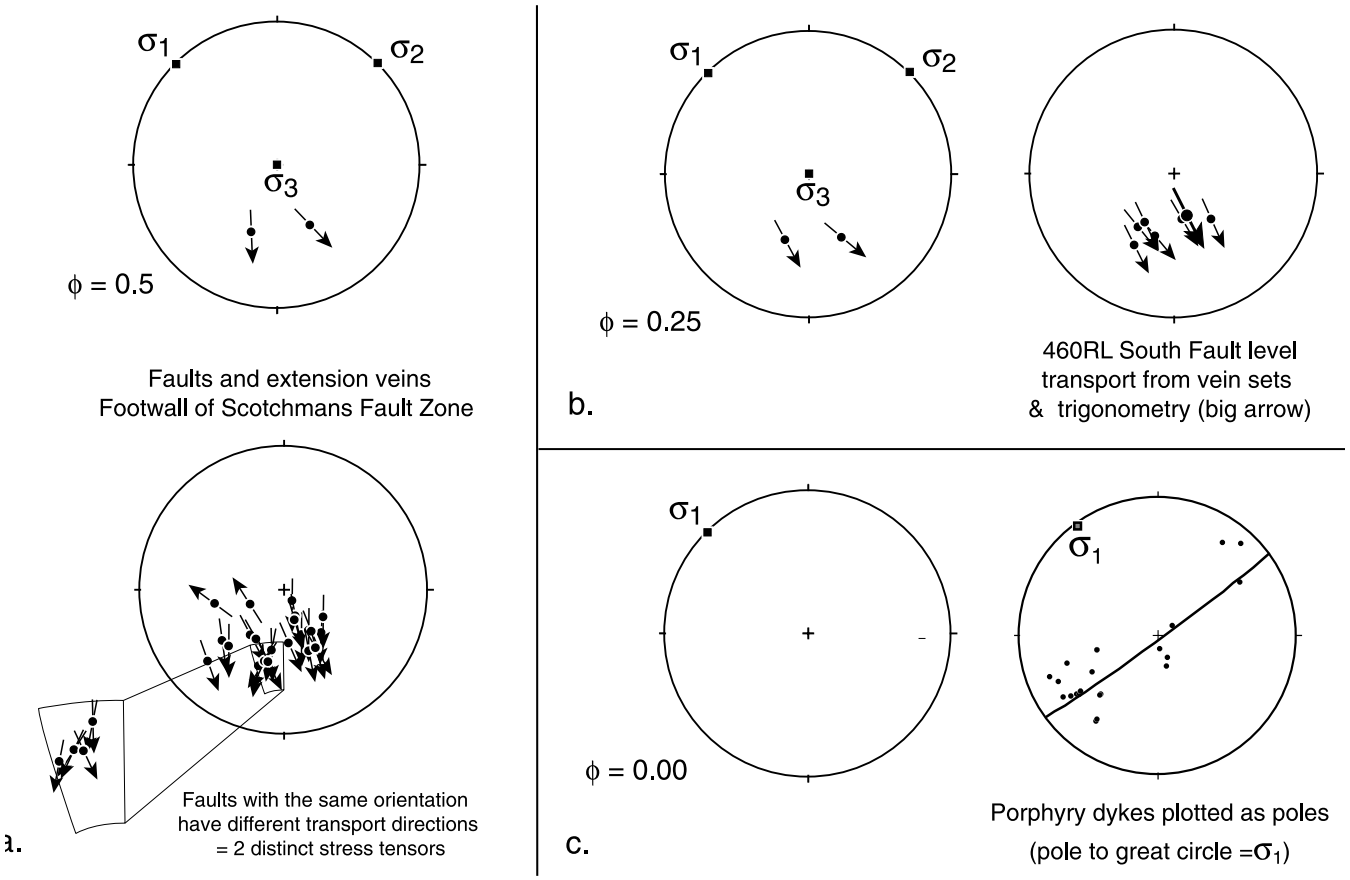

Fig. 20. Integration of porphyry dyke orientations with measured and calculated resolved shear stress data.

transport observed within the Scotchmans Fault Zone is the same age as the transport direction associated with the Wonga Lodes. Wonga-style ore does occur within the Magdala dome (particularly on the east flank). However, none of the extension veins associated with south-directed transport within Scotchmans Fault Zone have the distinct Wonga-style mineralogy.

5.3. Wonga mineralisation

The transport associated with the Wonga deposit does not match the dominant southeast-directed transport directions deduced from analysis of extension veins in the Scotchmans Fault Zone and direct hanging wall of the South Fault (Figs. 7, 13, 14). The deformation associated with the Wonga deposit also overprints a footwall crenulation cleavage related to northwest–southeast shortening (Fig. 16a). The deformation associated with the Wonga deposit has a close affinity to the Stawell pluton and the porphyry dykes and has frequently been termed a magmatic-associated or intrusion-related deposit (Bierlein et al., 2001; Miller and Wilson, 2002b). The massive veins and angular clasts of wall rock within the mineralised structures have been interpreted to represent a discrete fluid over pressure event (e.g. Wilson et al., 1999; Miller and Wilson, 2002b) rather than multiple crack-seal events (that are normally associated with laminated veins). There are not enough data to confidently assign a stress tensor to the Wonga deposit. However, the theoretical resolved shear stress diagrams highlight that the transport associated with the Wonga deposit cannot have occurred in a stress field with σ_1 flat-lying with an axis trending northwest–southeast (Fig. 17). The observed transport at Wonga could be related to σ_1 in a north–south orientation (Fig. 18).

5.4. South Fault

The data from the Wonga mine and the 460 RL of the Magdala Mine highlights that southwest-transport can be directly associated with the South Fault and is post the 413 Ma Porphyry dykes (Fig. 12a). At least some of the deformation is post contact metamorphism associated with the granodiorite phase of the Stawell pluton (Fig. 16b). At a larger scale the South Fault offsets contact metamorphism

Fig. 21. Summary of hanging wall transport data and inferred palaeostress directions (where possible) for all major brittle structures that post-date sinistral wrenching.

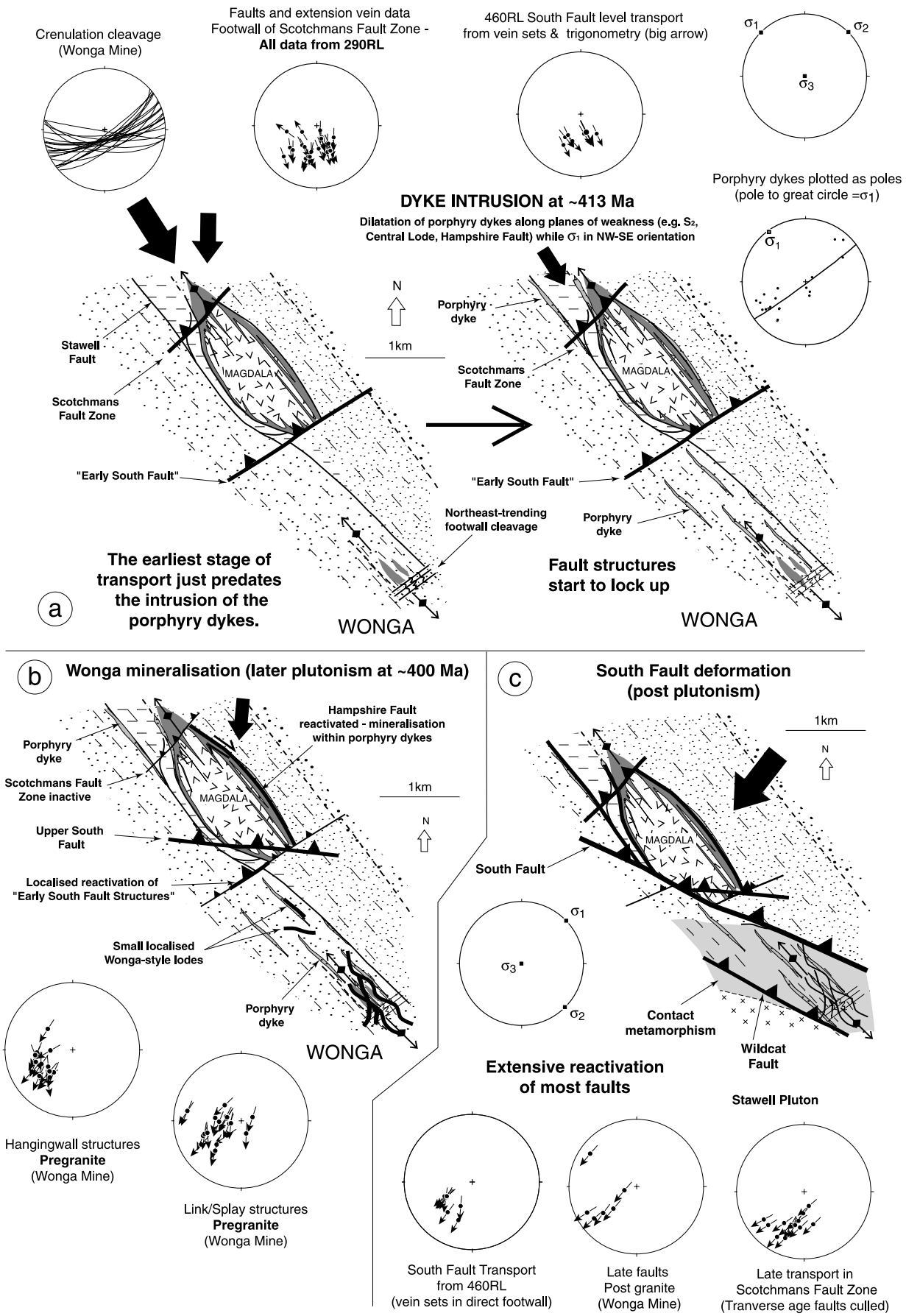
Crenulation cleavage
(Wonga Mine)
Faults and extension vein data
Footwall of Scotchmans Fault Zone -
All data from 290RL
460RL South Fault level transport
from vein sets & trigonometry (big arrow)
σ1
σ2
σ3
Porphyry dykes plotted as poles
(pole to great circle =σ1)
DYKE INTRUSION at ~413 Ma
Dilatation of porphyry dykes along planes of weakness (e.g. S2,
Central Lode, Hampshire Fault) while σ1 in NW-SE orientation
N
1km
Stawell
Fault
Scotchmans
Fault Zone
MAGDALA
"Early South Fault"
Northeast-trending
footwall cleavage
Porphyry
dyke
The earliest stage of
transport just predates
the intrusion of the
porphyry dykes.
Fault structures
start to lock up
WONGA
a
b
Wonga mineralisation (later plutonism at ~400 Ma)
Hampshire Fault
reactivated - mineralisation
within porphyry dykes
Porphyry
dyke
Scotchmans Fault
Zone inactive
Upper South
Fault
Localised reactivation of
"Early South Fault Structures"
Small localised
Wonga-style lodes
Hangingwall structures
Pregranite
(Wonga Mine)
Link/Splay structures
Pregranite
(Wonga Mine)
c
South Fault deformation
(post plutonism)
South Fault
Contact
metamorphism
Wildcat
Fault
Stawell Pluton
Extensive reactivation
of most faults
South Fault Transport
from 460RL
(vein sets in direct footwall)
Late faults
Post granite
(Wonga Mine)
Late transport in
Scotchmans Fault Zone
(Tranverse age faults culled)

associated with the granodiorite phase of the Stawell Pluton (Fredericksen and Gane, 1998; Miller et al., 2001). A comparison of striation data from the mapped regions indicates that the majority of faults have been reactivated during deformation associated with the South Fault.

In theory, the observed southwest-directed transport on faults with a South Fault orientation, and the south-directed transport on the similarly oriented hanging wall structures in the Wonga mine, could be related to a north–south oriented σ_1. Thus, all slip data could be related to the same stress tensor but with a relative change in σ_2 through time (i.e. $\phi = 0.25$ reflects south-directed Wonga mineralisation transport and $\phi = 0.75$ reflects southwest-directed South Fault age transport; Fig. 18). The use of compression and tension dihedra calculated from late striations measured on the 460 RL indicates σ_1 could have been oriented between north–south and northeast–southwest (Fig. 13). However, the extensive conjugate joints that occur in the direct hanging wall of the South Fault indicate that σ_2 was oriented northwest–southeast (Fig. 13). Furthermore, the use of SLICK.BAS for slickenside data from the 460 RL produced the same result for σ_2 (Fig. 13). Stress inversion of fault-slip data associated with striations from the 290 RL produced similar results (Fig. 7). However, for the 290 RL the orientation of σ_1 and σ_3 calculated using SLICK.BAS lay outside the fields predicted by the use of compression and tension dihedra. This indicates some heterogeneity in the slip data, although in all cases σ_2 was shallowly plunging to the northwest—in agreement with the conjugate joint data. All of the data suggest that the late southwest-directed movement on the faults was associated with a northeast–southwest oriented σ_1 with σ_2 flat-lying and to the southeast (Fig. 19). One interesting aspect of the orientation of these principal stresses is that it cannot produce the slip directions associated with Wonga age mineralisation.

5.5. Transverse reactivation and later transport

Late east- to east-northeast-trending faults termed 'Transverse Faults' occur throughout the Wonga Mine area. These faults dip steeply to the north and have a reverse movements sense with a component of dextral transport. In many areas late striations on graphitic fault surfaces indicate a hanging wall transport of top-to-the-southeast (e.g. on the actual south fault surface; Fig. 11). These are inferred to represent late transverse reactivation.

The final stage of brittle structures documented are a set of north–south striking reverse faults that dip steeply both east and west (e.g. stereonets; Fig. 14). This deformation may be associated with the strong reactivation of foliation surfaces observed within the Upper South Fault System (Fig. 8). These oblique striations are consistent with an east–west oriented σ_1.

5.6. Refinement of the existing geological framework

A change in regional stress within the Lachlan Fold Belt in the Late Silurian appears to have been preserved in the Stawell region. This is marked by a change from east–west shortening to sinistral wrenching along pre-existing faults; both of these structural events are associated with orogenic gold (Miller and Wilson, 2002a). This was followed by the formation of a major set of faults significantly oblique to earlier structural trends. These faults are associated with southeast-directed transport, and were termed 'early South Fault' structures by Miller et al. (2001) and have no gold association.

The 'early South Fault' structures regionally trend to the northeast on total magnetic intensity images and have been mapped underground and on the surface at Stawell, Ararat (Copes Hill road cutting and Carroll's cutting; fig. 12b and e of Phillips et al., 2002) and also at Mount Drummond within the adjacent Delamerian Fold Belt (fig. 8a of Miller et al., 2002). These structures have been correlated with deformation of the Silurian Grampians Group and also changes in sedimentation within the Melbourne Trough (Miller et al., 2001; now the Melbourne Zone; Fig. 1a).

The 'early South Fault' structures correspond to the initial stages of transport along Scotchmans Fault Zone and the faults that underlie the currently mined part of the Magdala orebody (Fig. 21a). This set of faults also appears to be associated with northeast- and east-northeast-trending cleavages (observed in the Wonga Mine; Figs. 14, 16a and 21a) that are oblique to earlier fabrics (i.e. S_2, S_3). At the Magdala Mine porphyry dykes have intruded along these faults after substantial southeast-directed transport occurred (Miller et al., 2001). The observed slip directions documented by analysis of footwall extension veins does not require an extensive variation in the orientation of the principal stresses. These data are consistent with compression related to a palaeostress associated with a flat-lying σ_1 oriented northwest–southeast (Fig. 21a). There appears to have been a gradual reduction in σ_2 associated with dyke emplacement representing the end stage of the observed geological history associated (Fig. 21c).

The Wonga lodes are structurally and mineralogically distinct and have been related to the intrusion of the Stawell pluton (Wilson et al., 1999; Bierlein et al., 2001; Miller and Wilson, 2002b). Regional gold-mineralisation that occurs within diorite bodies is inferred to be the same age (e.g. the White Rabbit diorite; Cayley and Taylor, 2001; Fig. 1b). The Wonga Lodes overprint the porphyry dykes and the footwall crenulation cleavages related to northwest–southeast shortening. The transport associated with the Wonga Lodes does not match the inferred palaeostress directions for either the 'early South Fault structures' or the South Fault aged structures. The available data indicate that the Wonga lodes formed as a result of a discrete fluid over pressure event after the lockup of major structures that transported units to the southeast and south-southeast ('early

South Fault' structures and emplacement of the porphyry dyke intrusions) and prior to major southwest-directed transport of units in the hanging wall of the South Fault post the intrusion of the Stawell granodiorite (Fig. 21b).

The last major stage of deformation appears to be associated with what are termed 'South Fault-age' structures with the calculated orientation of σ_1 flat-lying and oriented northeast–southwest (Fig. 21c). These faults occur regionally, throughout the Stawell mine and consistently dip to the northwest with dip-slip movement. These faults are inferred to represent neoformed faults (i.e. they formed and moved dominantly in a single stress regime). Much of the alteration and transport along these faults is post plutonism (<400 Ma). 'South Fault aged' deformation also occurs within Devonian hornfels in the adjacent Delamerian orogen (Miller et al., 2002). At one locality in the Delamerian Fold Belt they have been demonstrated to have a conjugate geometry consistent with a northeast–southwest oriented σ_1 and northwest–southeast σ_2 (fig. 8a of Miller et al., 2002). These 'South Fault aged' faults have been correlated with the distinct Tabberabberan orogeny (Miller et al., 2001), which has been documented throughout the Lachlan Fold Belt.

There is a change in hanging wall transport from southeast- to south- and then southwest-directed depicted on Fig. 21. However, this does not appear to reflect progressive deformation associated with a gradual rotation of the σ_1 stress orientation from northwest–southeast to north–south and then northeast–southwest. The end stage of transport along the 'early South Fault' structures is marked by the intrusion of the porphyry dykes (~413 Ma; Arne et al., 1998). The next major phase of regionally documented deformation (i.e. South Fault age structures and reactivation of earlier faults) is post the Devonian batholiths (~401 Ma; Arne et al., 1998). These plutons are generally massive with no internal foliation and are not typical of syntectonic plutonism. The Wonga deposit is inferred to reflect the stress distribution around the Stawell pluton at the time of intrusion-related fluid overpressure and does not correlate with any regional deformation. Even the assumption that the principal stresses were vertical and flat-lying for this phase of magmatic associated mineralisation may not hold. There was at least 10–15 million years between the two deformations that had regional extent.

6. Conclusions

The complex fault relationships documented in the Stawell region highlight that the best approach when mapping within such systems is to systematically map striations and footwall/hanging wall extension veins and joint sets (e.g. conjugate joints). In the case of the Golden Gift orebody, the extension veins record an earlier history of fault transport that was not preserved by striations. While the calculation of net transport vectors is desirable, only two conclusive examples were found from the entire Stawell system during 10 months of underground mapping. Furthermore, net transport vectors do not give a picture of the entire movement history on a fault.

Diagrams of theoretical maximum resolved shear stress are a valuable tool that allow consideration of a range of possible palaeostresses for a given fault slip data set, rather than attempting to assign a single stress tensor. Even in an area as structurally complex as Stawell, the application of multiple structural methods (compression and tension dihedra, stress inversion of slip data, use of conjugate joints/faults and theoretical shear stress calculations) makes it possible to delineate a reasonable palaeostress history. The calculation of actual ϕ values is not always possible, though an understanding of the implication of varying this value for slip directions is important in interpreting fault slip data associated with non-Andersonian geometries when delineating a possible palaeostress history.

Acknowledgements

This research has been funded by an Australian Research Council SPIRT Grant, Mining Project Investors Pty Ltd and the Predictive Mineral Discovery Cooperative Research Centre. The directors of Mining Project Investors Pty Ltd are thanked for allowing publication prior to the expiration of a confidentiality agreement. We acknowledge the great help provided by numerous company staff, in particular, J. Dugdale, D. Fredericksen, G. McDermott, J. Moncrieff and A. Bourke. This paper is published with the permission of the CEO of the Predictive Mineral Discovery Cooperative Research Centre. Editorial comments by Tom Blenkinsop and constructive reviews by Neil Phillips and Richard Lisle substantially improved the manuscript.

References

Anderson, E.M., 1951. The Dynamics of Faulting. Oliver and Boyd, Edinburgh, 206pp.

Andrew, A.S., Gulson, B.L., Carr, G.R., Keays, R., 2002. Victorian hardrock gold deposits: sources and sinks. In: Phillips, G.N., Ely, K.S. (Eds.), Victoria Undercover Benalla, 2002. Conference Proceeding and Field Guide, pp. 71–78.

Angelier, J., 1984. Tectonic analysis of fault slip data sets. Journal of Geophysical Research 89, 5835–5848.

Angelier, J., 1994. Fault slip analysis and palaeostress reconstruction. In: Hancock, P.L., (Ed.), Continental Deformation, Pergamon, Oxford, pp. 53–100.

Arne, D.C., Bierlein, F.P., McNaughton, N., Wilson, C.J.L., Morand, V.J., 1998. Timing of gold mineralization in western and central Victoria, Australia: new constraints from SHRIMP II analysis of zircon grains from felsic intrusive rocks. Ore Geology Reviews 13, 251–273.

Bierlein, F.P., Arne, D.C., Keay, S.M., McNaughton, N.J., 2001. Timing relationships between felsic magmatism and mineralisation in the central Victorian gold province. Australian Journal of Earth Sciences 48, 883–899.

Bird, P.J., 1986. Tectonic and Intrusive Geological History of the Great

Western-Stawell Area: Central Western Victoria: B.Sc. (hons.) thesis, Latrobe University (unpub.).

Cayley, R.A., Taylor, D.H., 2000. STAWELL 1:50000 Map sheet, 7423-1, Geological Survey of Victoria.

Cayley R.A. Taylor D.H., 2000. ARARAT 1:50000 Map sheet, 7432-2, Geological Survey of Victoria.

Cayley, R.A., Taylor, D.H., 2001. Geological survey report for the Ararat 1:100000 map sheet. Geological Survey of Victoria Report, no. 121.

Cox, S.F., Etheridge, M.A., Cas, R.A.F., Clifford, B.A., 1991. Deformation style of the Castlemaine area, Bendigo–Ballarat Zone: implications for the evolution of crustal structure in central Victoria. Australian Journal of Earth Sciences 38, 151–170.

Cox, S.F., Sun, S.-S., Etheridge, M.A., Wall, V.J., Potter, T.F., 1995. Structural and geochemical controls on the development of turbidite-hosted gold quartz vein deposits, Wattle Gully Mine, Central Victoria, Australia. Economic Geology 90, 1722–1746.

Cox, S.F., Ruming, Nguyen, P.T., Stone, W.E. 2001. The behaviour of faults, fluids and gold in a crustal scale shear system, St Ives Goldfield WA—a case of Golden aftershocks? In: Davidson, G., Pongratz, J. (Eds.), 2001: A Structural Odyssey. Specialist Group in Tectonics and Structural Geology, February 2001, Ulverstone, Australia. Geological Society of Australia Abstracts Volume 64, p. 28.

Dugdale, L.J., Fredericksen, D., 2000. Exploration success at Stawell. Discovery. Earth Science Journal of the Victorian Department of Natural Resources and Environment February, 2–4.

Fergusson, C.L., Gray, D.R., Cas, R.A.F., 1986. Overthrust terranes in the Lachlan Fold Belt, southeastern Australia. Geology 14, 519–522.

Foster, D.A., Gray, D.R., Kwak, T.A.P., Bucher, M., 1998. Chronology and tectonic framework of turbidite hosted gold deposits in the western Lachlan Fold Belt, Victoria: $^{40}Ar-^{39}Ar$ results. Ore Geology Reviews 13, 229–250.

Fredericksen, D.C., Gane, M., 1998. Stawell gold deposit. In: Berkman, D.A., Mackenzie, D.H. (Eds.), Geology of Australian and Papua New Guinean Mineral Deposits, The Australasian Institute of Mining and Metallurgy, Melbourne, pp. 535–542.

Fry, N., 1992. Direction of shear. Journal of Structural Geology 14, 253–255.

Gómez, S.J.-L., 1986. Analysis of the gradual change in stress regime (example for the eastern Iberian Chain, Spain). Tectonophysics 124, 37–53.

Gray, D.R., 1988. Structure and tectonics. In: Douglas, J.G., Ferguson, J.A. (Eds.), Geology of Victoria, Geological Society of Australia, Victorian Division, Melbourne, pp. 1–36.

Groves, D.I., Goldfarb, R.J., Knox-Robinson, C.M., Ojala, J., Gardoll, S., Grace, Y.Y., Holyland, P., 2000. Late-kinematic timing of orogenic gold deposits and significance for computer-based exploration techniques with emphasis on the Yilgarn Block, Western Australia. Ore Geology Reviews 17, 1–38.

Hoeppener, R., 1955. Tektonik im Schieferbirge. Geologische Rundschau 44, 26–58.

Holyland, P.W., Ojala, V.J., 1997. Computer aided structural targeting in mineral exploration: two and three-dimensional stress mapping. Australian Journal of Earth Sciences 44, 421–432.

Lisle, R.J, S., Vandycke, S., 1996. Separation of multiple stress events by fault striation analysis: an example from Variscan and younger structures at Ogmore, South Wales. Journal of the Geological Society, London 153, 945–953.

Miller, J.McL., Wilson, C.J.L., 2002a. The Magdala Lode System, Stawell, southeastern Australia: structural style and relationship to gold mineralisation across the western Lachlan Fold Belt. Economic Geology 97, 325–349.

Miller, J.McL., Wilson, C.J.L., 2002. Differential stress controls on gold lode formation during intrusion-related fluid overpressure, Wonga Mine, Western Lachlan Fold Belt, Australia. In: Verncombe, S. (Ed.), Applied Structural Geology for Mineral Exploration and Mining. International symposium, Kalgoorlie, Western Australia. Australian Institute of Geoscientists Bulletin 36, pp. 135–137.

Miller, J.McL., Dugdale, L.J., Wilson, C.J.L., 2001. Variable hanging wall palaeotransport during Silurian and Devonian thrusting in the Lachlan Fold Belt—missing gold lodes, synchronous Melbourne Trough sedimentation and Grampians Group fold interference. Australian Journal of Earth Sciences 48, 901–909.

Miller, J.McL., Norvick, M.S., Wilson, C.J.L., 2002. Basement controls on rifting and the associated formation of ocean transform faults–Cretaceous continental extension of the southern margin of Australia. Tectonophysics 359, 131–155.

Oncken, O., 1988. Aspects of the reconstruction of the stress history of a fold and thrust belt (Renish Massif. Federal Republic of Germany). Tectonophysics 152, 19–40.

Phillips, G.N., Hughes, M.J., 1998. Victorian gold province. In: Berkman, D.A., Mackenzie, D.H. (Eds.), Geology of Australian and Papua New Guinean Mineral Deposits, The Australasian Institute of Mining and Metallurgy, Melbourne, pp. 495–506.

Phillips, G., Miller, J.McL., Wilson, C.J.L., 2002. Structural and metamorphic evolution of the Moornambool Metamorphic Complex, western Lachlan Fold Belt, southeastern Australia. Australian Journal of Earth Sciences 49, 891–913.

Ramsay, J.G., Huber, M.I., 1987. The Techniques of Modern Structural Geology. Volume 2: Fold and Fractures, Academic Press, London, pp. 309–700.

Ramsay, J.G., Lisle, R., 2000. The Techniques of Modern Structural Geology. Volume 3: Applications of Continuum Mechanics in Structural Geology, Academic Press, San Diego, USA, pp. 701–1061.

Robert, F., Poulsen, K.H., 2001. Vein formation and deformation in greenstone gold deposits. Society of Economic Geologists, Reviews 14, 111–155.

Robert, F., Boullier, A.-M., Firdaous, K., 1995. Gold–quartz veins in metamorphic terranes and their bearing on the role of fluids in faulting. Journal of Geophysical Research 100, 12861–12879.

Sibson, R.H., Scott, J., 1998. Stress/fault controls on the containment and release of overpressured fluids: examples from gold–quartz vein systems in Juneau, Alaska, Victoria, Australia and Otago, New Zealand. Ore Geology Reviews 12, 293–306.

Sibson, R.H., Robert, F., Poulsen, K.H., 1988. High-angle reverse faults, fluid-pressure cycling, and mesothermal gold–quartz deposits. Geology 16, 551–555.

Watchorn, R.B., Wilson, C.J.L., 1989. Structural setting of gold mineralization at Stawell, Victoria, Australia. In: The Geology of Gold Deposits: The Perspective in 1988. Economic Geology Monograph 6, pp. 292–309.

Wilson, C.J.L., Will, T.M., Cayley, R.A., Chen, S., 1992. Geological framework and tectonic evolution in western Victoria, Australia. Tectonophysics 214, 93–127.

Wilson, C.J.L., Xu, G., Moncrieff, J., 1999. The structural setting and contact metamorphism of the Wonga gold deposit, Victoria, Australia. Economic Geology 94, 1305–1328.

Xu, G., Powell, R., Wilson, C.J.L., Will, T., 1994. Contact metamorphism around the Stawell granite, Victoria, Australia. Journal of Metamorphic Petrology 12, 609–624.